The impact of metastable intermolrecular nanocomposite particles on kinetic decomposition of heterocyclic nitramines using advanced solid-phase decomposition models

Sherif Elbasuney (sherif_basuney2000@yahoo.com)
Military Technical College (MTC), Cairo, Egypt
Abdelaziz Hamed
Military Technical College (MTC), Cairo, Egypt
M. Yehia
Military Technical College (MTC), Cairo, Egypt
Hesham Ramzy
Military Technical College (MTC), Cairo, Egypt
Ahmed Abdelgawad
Military Technical College (MTC), Cairo, Egypt
Mohamed Gobara
Military Technical College (MTC), Cairo, Egypt
Mohamed Mokhtar
Military Technical College (MTC), Cairo, Egypt

Research Article

Keywords: Kinetic study, Nanocatalyst, Nanothermites, Energetic materials, Nanoparticles

Posted Date: February 15th, 2021

DOI: https://doi.org/10.21203/rs.3.rs-237962/v1

The impact of metastable intermolrecular nanocomposite particles on kinetic decomposition of heterocyclic nitramines using advanced solid-phase decomposition models

Sherif Elbasuney [a, b*], Abdelaziz Hamed [b], M. Yehia [b], Hesham Ramzy [b], Ahmed Abdelgawad [b], Mohamed Gobara [b], Mohamed Mokhtar [b]

[a] Head of Nanotechnology Research Center, Military Technical College (MTC), Cairo, Egypt.
[b] School of Chemical Engineering, Military Technical College (MTC), Cairo, Egypt.

*Corresponding authors: s.elbasuney@mtc.edu.eg, sherif_basuney2000@yahoo.com

[a] School of Chemical Engineering, Military Technical College, Cairo, Egypt.

[b] Head of Nanotechnology Research Center, Military Technical College, Cairo, Egypt.

s.elbasuney@mtc.edu.eg, sherif_basuney2000@yahoo.com

Abstract

Oxygen atoms on the surface of oxide catalysts have low coordination number; they are negatively charged. Surface oxygen can act active sites for decomposition of energetic nitramines (i.e. HMX); additionally hydrous surface can release active ȮH radicals. Colloidal oxide particles can fulfil these requirements. Furthermore oxide particles can induce thermite reaction with aluminium particles. This study reports on the facile fabrication of colloidal ferric oxide particles of 5 nm; Colloidal Fe_2O_3/Al binary mixture was integrated into HMX matrix via co-precipitation technique; uniform dispersion of nanothermite particles was verified using SEM. Naonothermite particles experienced dramatic change in HMX thermal behaviour with an increase in total heat release by 63 %. The impact of themrite particles on HMX kinetic decomposition was evaluated using an integral isoconversional method of KAS, and Kissinger models. The mean value of apparent activation was reduced by 23.5 % and 24.3 % using Kissinger and KAS models respectively. This dramatic change in HMX decomposition can be ascribed to the ferric oxide reactivity and the facile integration of colloidal thermite particles.

Keywords: Kinetic study; Nanocatalyst; Nanothermites; Energetic materials; Nanoparticles.

1. Introduction

Energetic nanocomposite materials are emerging class of materials with adapted performance in terms of sensitivity, decomposition enthalpy, kinetic decomposition parameters (i. e. activation energy) [1-3]. Energetic nitramines (i. e. RDX, HMX, Cl20) are attractive materials in terms of power (strength), high chemical stability, and stability (Figure 1).

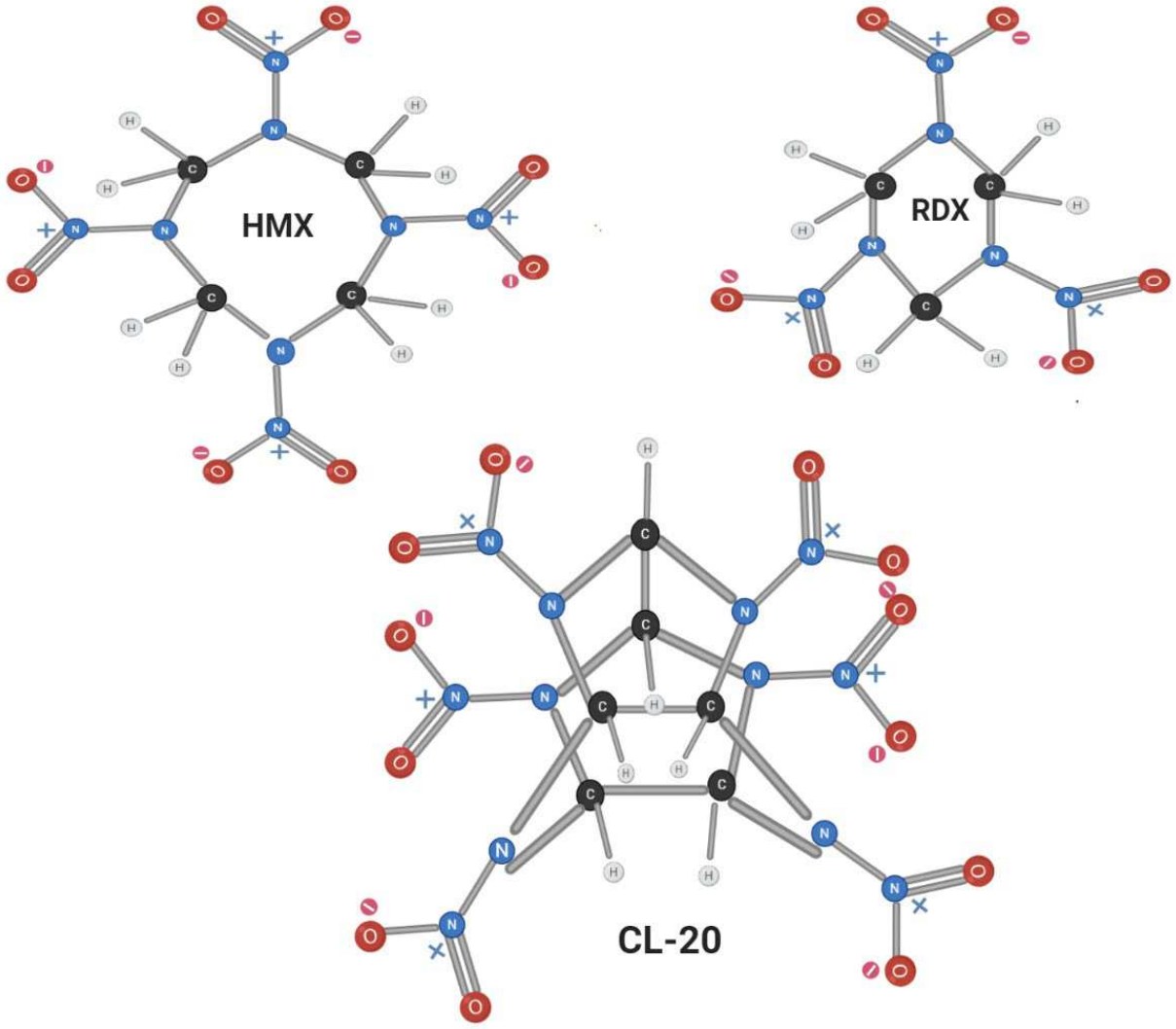

Fig. 1: Chemical structure of common energetic nitramines [4].

Optimization between performance and sensitivity is a crucial issue [5-7]. HMX is one of the most vigorous energetic nitramines; however the performance of energetic materials is limited to hydrocarbon combustion [8-9]. One of the most common oxidizer for nanothermite applications is ferric oxide. Ferric oxide can act catalyst for hetrocyclic nitramines; oxygen atoms on the surface of ferric oxide can experience low coordination; and have unique electron donor properties [10]. These electron donor sites can site of induce catalytic decomposition of electron deficient energetic nitramines [11]. Additionally ferric oxide can experience hydrous surface; free ȮH radical can be evolved and attack nitramine heterocyclic ring [2, 11-12]. Colloidal particles can secure hydrous surface. There is a potential for fabrication technology that could offer fabrication of ferric oxide particles in dispersion. Hydrotherthaml processing can secure such requirements. Hydrothermal processing has an edge over all other classical synthesis techniques such as ball milling, sintering, and firing (Figure 2).

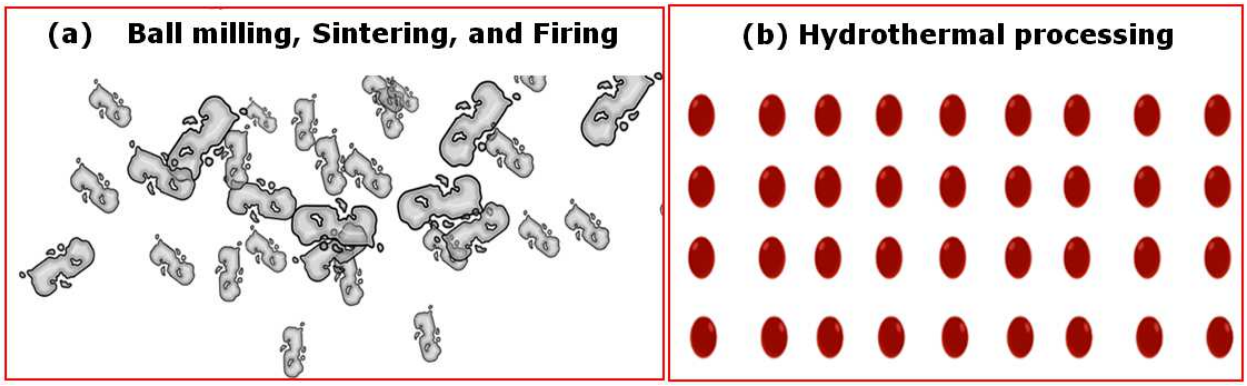

Fig. 2: Nanoparticles morphology produced by different methods [13-15].

Hydrothermal processing can secure mono-dispersed particles free from defects with high crystalline structure, controlled geometry [16-17].Further details about hydrothermal processing can be found in the following literatures [18-19]. Nanothermite particles can offer low critical diameter, enhanced initiability, low activation energy, high reaction propagation[20-24]. Furthermore nanothermite particles can experience dramatic change in decomposition kinetics. Thermal behaviour and kinetics of the

energetic materials is essential for the prediction of the process rate and knowing the material life time. Different thermal analysis techniques can be adopted for thermal decomposition study i.e. TGA, DTA, and DSC. Kinetic parameters i. e. activation energy, preexponential factor, and the model of the reaction can be evaluated Equation 1.

$$\frac{d\alpha}{dt} = k(T)f(\alpha) \qquad (1)$$

Where $\frac{d\alpha}{dt}$, is the rate of reaction, $k(T)$ is the absolute temperature, and $f(\alpha)$ is the solid state reaction model. Isconversional model is based on the principle that at constant fraction reacted; the reaction rate is only function of temperature (Equation 2).

$$\left[\frac{\partial \ln\left(\frac{d\alpha}{dt}\right)}{\partial T^{-1}}\right]\alpha = \left[\frac{\partial \ln k(T)}{\partial T^{-1}}\right]\alpha + \left[\frac{\partial \ln f(\alpha)}{\partial T^{-1}}\right]\alpha \qquad (2)$$

Second term of the equation (2) would be zero by applying first derivative. Finally, activation energy could be determined straightforward from the slope of the plot (Equation 3).

$$\left[\frac{\partial \ln\left(\frac{d\alpha}{dt}\right)}{\partial T^{-1}}\right]\alpha = -\frac{E\alpha}{R} \qquad (3)$$

Where α is the extent of conversion, E_α is the apparent activation energy, and R is the universal gas constant. The current study reports on the facile development of colloidal nanothermite particles and effective integration of themrite particles into energetic nitramine matrix (HMX). The impact of thermite particles on HMX thermal behaviour was evaluated. The impact of themrite particles on HMX kinetic decomposition was evaluated using an integral isoconversional method of KAS, and Kissinger models. The mean value of apparent activation was reduced by 23.5 % and 24.3 % using Kissinger and KAS models respectively. This dramatic change in HMX decomposition can be ascribed to the high reactivity of Fe_2O_3 NPs and the facile integration of colloidal thermite particles.

2. Experimental work

2.1 Characterization of thermite particles

Morphology (shape and size) of ferric oxide and aluminium nanoparticles was investigated using TEM (JEM-2100F by Joel Corporation). The dry powder size and shape was investigated with SEM ZEISS SEM EVO 10 MA.

2.2 Formulation of HMX nanocomposite

It is widely accepted that the integration of colloid particles into energetic matrix can secure high dispersion levels [25]. Colloidal Fe_2O_3 particles were harvested from their synthesis medium and re-dispersed in acetone. Aluminum NPs were dispersed in acetone collid; consequently HMX was dissolved. HMX nanocomposite was developed via proper anti-solvent. The precipitate was filtered and dried (Figure 3).

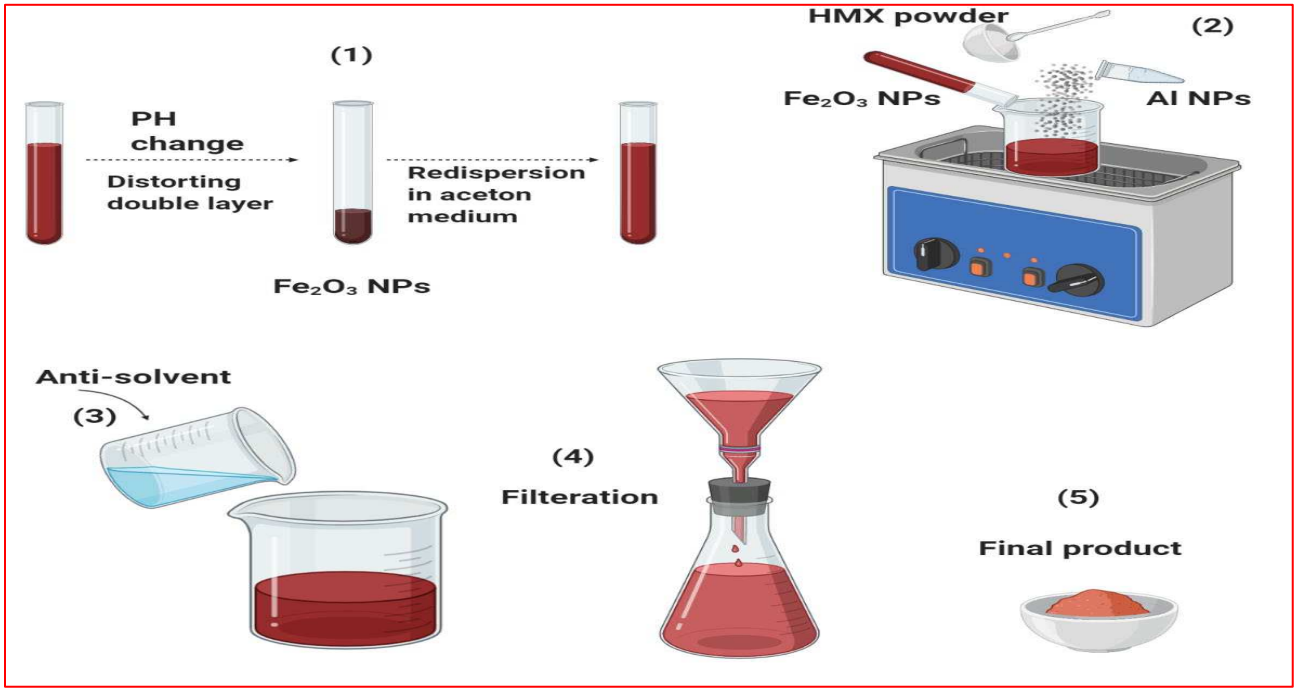

Fig. 3: Solvent anti-solvent technique for preparation of HMX nanocomposite

Morphology of developed HMX nanocomposite was investigated using SEM. Furthermore dispersion level of thermite particles into energetic matrix was investigated using EDAX detector.

2.3 Thermal behaviour of HMX nanocomposite

Thermal behaviour of HMX nanocomposite was investigated by DSC Q20 by TA, USA. The tested sample was heated at 5 °C min^{-1} up to 500 °C, under N_2 gas flow of 50 ml min^{-1}.

2.4 Decomposition Kinetics of HMX nanocomposite

Isoconversional (model free) and model fitting are the two main models to study decomposition kinetics. Decomposition kinetic parameters were evaluated by two models including isoconvertional method of KAS, and Kissinger models respectively. Activation energy of HMX nanocomposite was evaluated and compared to the value of pure HMX. DSC experiments were conducted at three different heating rates 2, 3, and 5 °C·min^{-1}.

2.4.1 Integral isconversional model

Integral methods are driven from the integration of Equation 4:

$$g(\alpha)=\int_0^{\alpha}\frac{d\alpha}{f(\alpha)}=A\int_0^{t}e^{\wedge}\left(-\frac{E}{RT}\right)dt \qquad (4)$$

Where g(α) is the integral form of the reaction model. At constant heating rate there is no analytical solution; consequently there is a number of integral isoconversional methods that have different approximation of the temperature integral in Equation (5) [26].

$$g(\alpha)=\frac{A}{\beta}\int_0^{T}e^{\wedge}\left(-\frac{E}{RT}\right)dT \qquad (5)$$

Where β is the heating rate; A is the pre-exponential factor. In this manuscript the integral isoconvertional method of Kissinger-Akahira-Sunose (KAS) equation (6) has been adopted for activation energy calculation.

$$\ln\left(\frac{\beta i}{T\alpha,i^{1.92}}\right) = const - 1.0008\left(\frac{E\alpha}{RT\alpha}\right) \quad (6)$$

2.4.2 Kissinger model

Kissinger model is a straight forward method with wide applications [27]. The equation from this method has been driven from equation (1) and the condition was the maximum reaction rate and at this point $\frac{d^2\alpha}{dt^2} = 0$ as presented in equation (7).

$$\frac{d^2\alpha}{dt^2} = \left[\frac{E\beta}{RTm^2} + Af'(\alpha_m)\exp\left(-\frac{E}{RTm}\right)\right]\left(\frac{d\alpha}{dt}\right)_m = 0 \quad (7)$$

After rearrangement equation (7) becomes equation 8

$$\ln\left(\frac{\beta}{Tm,i^2}\right) = \ln\left(-\frac{AR}{E}f'(\alpha_m)\right) - \frac{E}{RTm,i} \quad (8)$$

Prior to apply this model the fraction reacted at maximum rate should be constant at the three different heating rates. Activation energy can be evaluated from the slope of the straight line of $\ln\left(\frac{\beta}{Tm,i^2}\right)$ versus $\left(\frac{1}{Tm}\right)$.

3. Results and Discusssions

3.1 Characterization of thermite particle

TEM micrographs demonstrated mono-dispersed Fe_2O_3 nanoparticles of a particle size of 5 nm (Figure 4-a). Highly crystalline structure is confirmed from incident beam diffraction (Figure 4-b). Aluminium nanoplates of 100 nm were confirmed (Figure 4-c). Highly crystalline material is confirmed from incident bean diffraction (Figure 4-d).

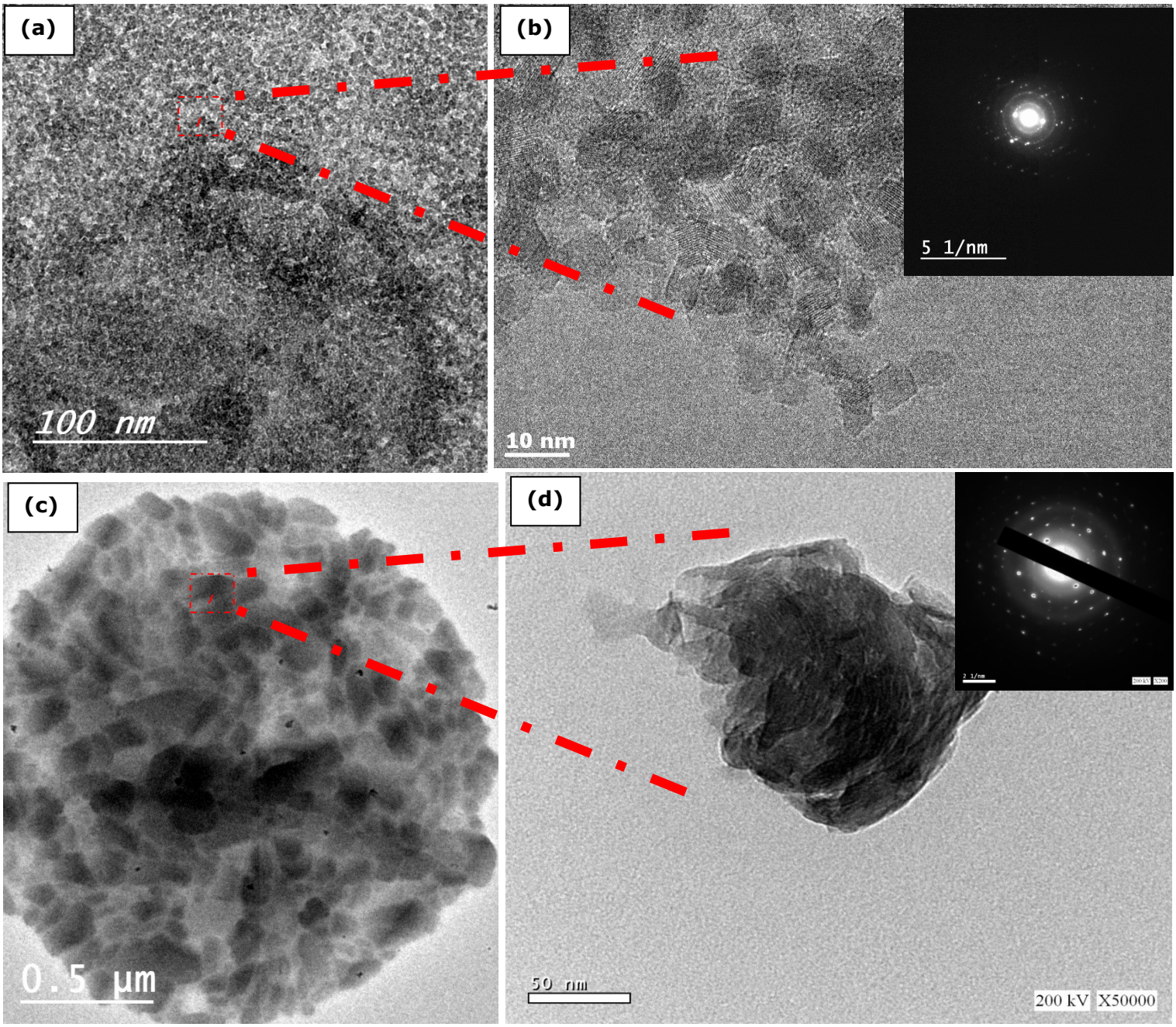

Fig. 4: TEM for the synthesized Fe_2O_3 nanoparticles (a, b) and aluminium nanoparticles (c, d).

SEM micrographs of dry Fe_2O_3 particles demonstrated high affinity to decrease their number and surface area (Figure 5 a-b). Aluminium flakes were reported from SEM micrographs (Figure 5 c-d).

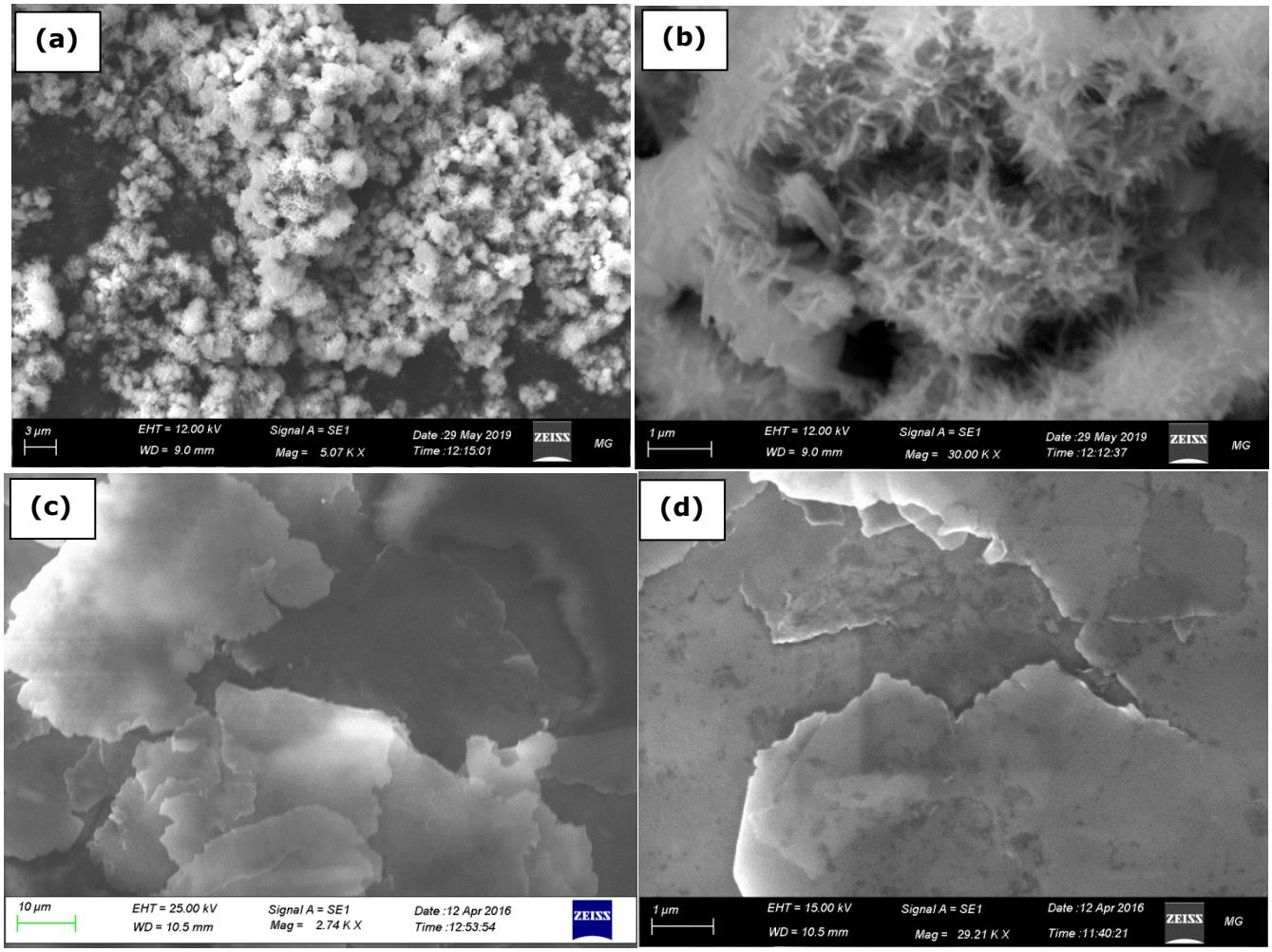

Fig. 5: SEM micrograhs Fe_2O_3 nanoparticles (a, b), aluminium nanoplates (c, d).

There a great potential to integrate colloidal particles into different energetic matrix can eliminate integration of dry aggregates. Therefore superior particle dispersion could be accomplished.

3.2 Characterization HMX nanocomposite

Size and shape of HMX nanocomposite was investigated with SEM; SEM micrographs demonstrated cubic crystals with average particle size of 5 µm (Figure 6). Uniform dispersion of nanothermite particles is obvious.

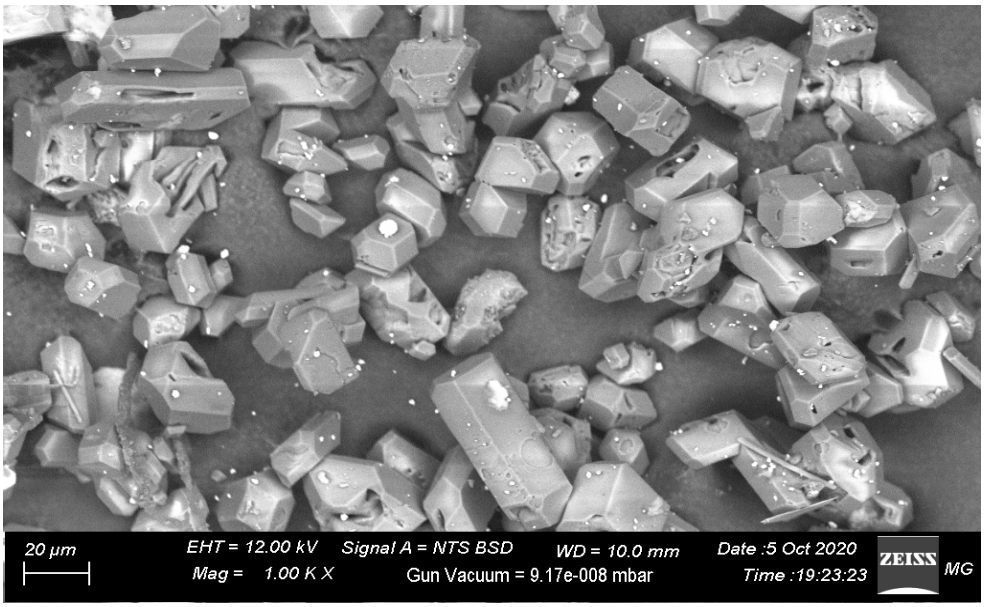

Fig. 6: Morphology of HMX nanocomppsoite

Elemental mapping using EDAX detector confirmed good dispersion of thermite particles. Moreover, the even dispersion of main element Al, Fe, O, N is obvious (Figure 7).

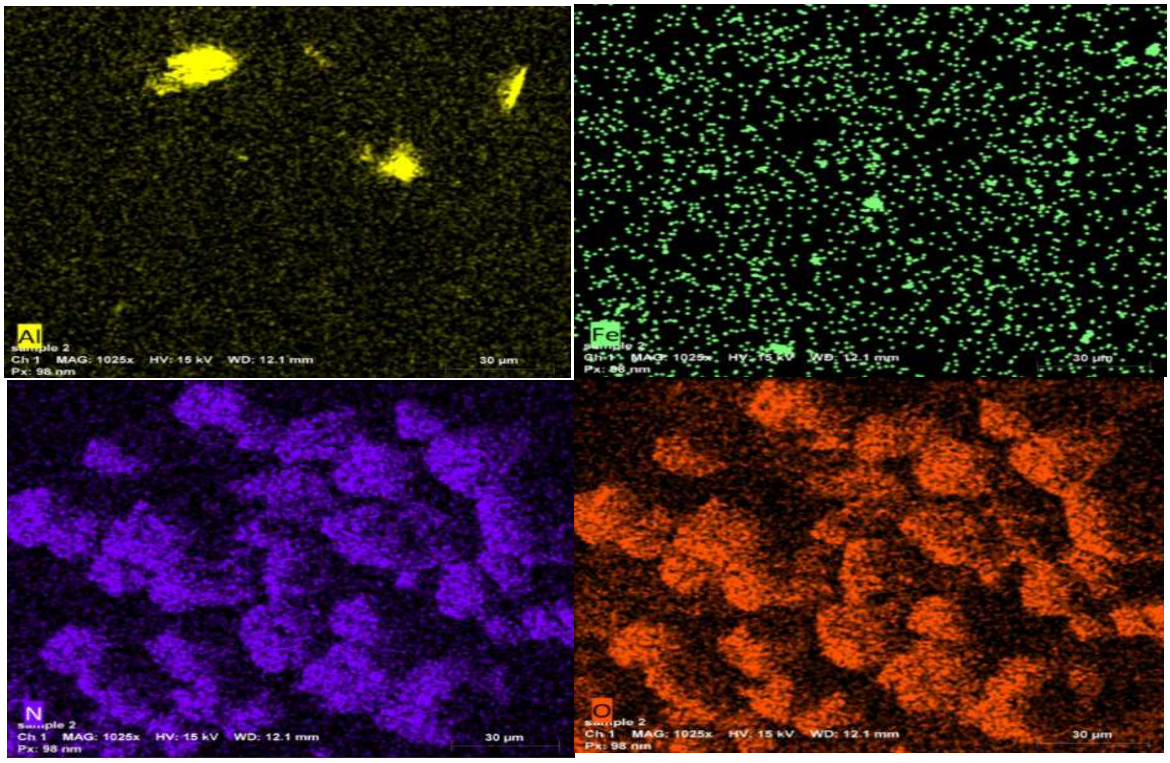

Fig. 7: Elemental mapping of HMX nanocomposite

Elemental analysis confirmed the existence of main component in right percentage (Figure 8).

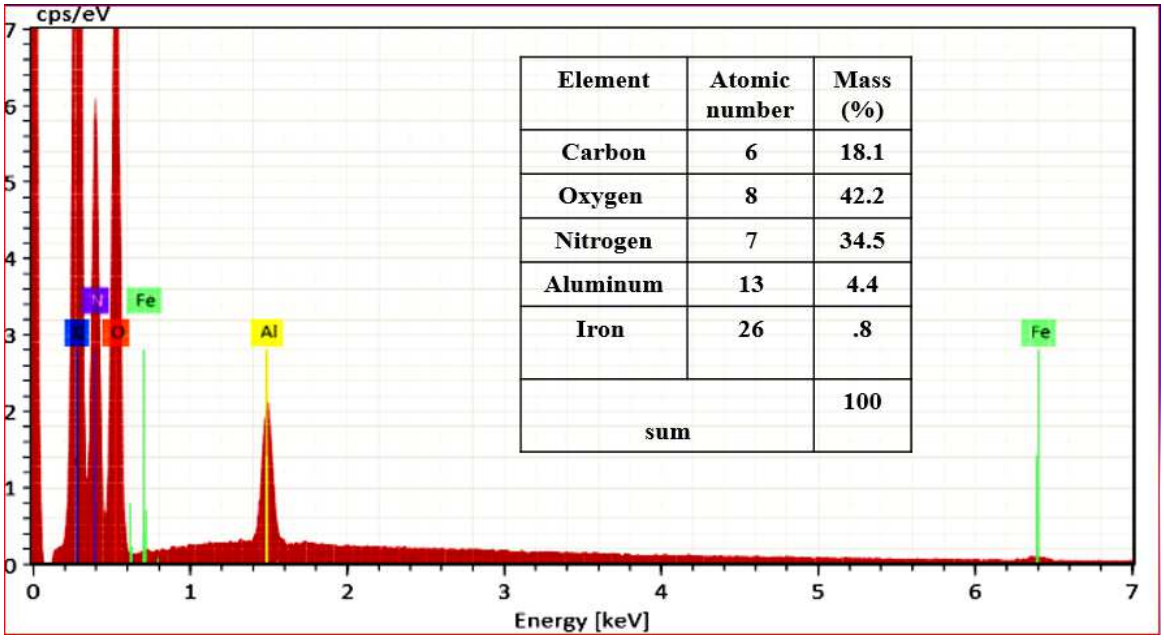

Element	Atomic number	Mass (%)
Carbon	6	18.1
Oxygen	8	42.2
Nitrogen	7	34.5
Aluminum	13	4.4
Iron	26	.8
sum		100

Fig. 8: EDX elemental analysis of HMX nanocomposite.

Elemental analysis confirmed the absence of any interfering impurities. It can be concluded that proper integration of colloidal thermite particles into energetic matrix has been accomplished.

3.3 Thermal behaviour of HMX nanocomposite

Integration of thermite nanoparticles into HMX matrix demonstrated superior change in the thermal behaviour (Figure 9).

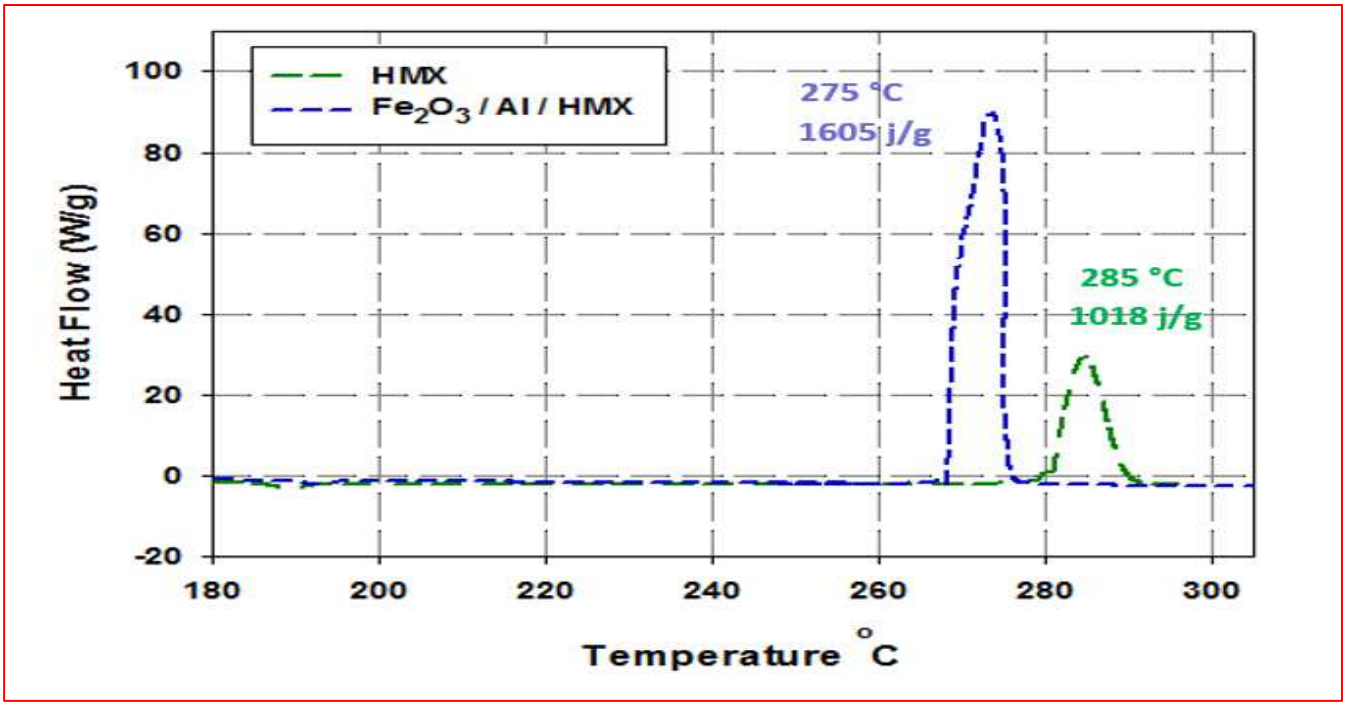

Fig. 9: Impact of thermite particles on HMX thermal behaviour.

Nanothermites offered an increase in the total heat release by 63 %. Furthermore the maximum decomposition temperature has been decreased by 10 °C.

3.4 Kinetic decomposition of HMX nanocomposite

Main kinetic decomposition parameters and activation energy were evaluated using KAS and Kissinger models respectively. HMX nanocomposite were heated at different heating rates of 2, 3, 5 ^{0}C min^{-1} using DSC (Figure 10). It is widely accepted that optimum operation conditions include low heating rate, to minimize heat losses [28].

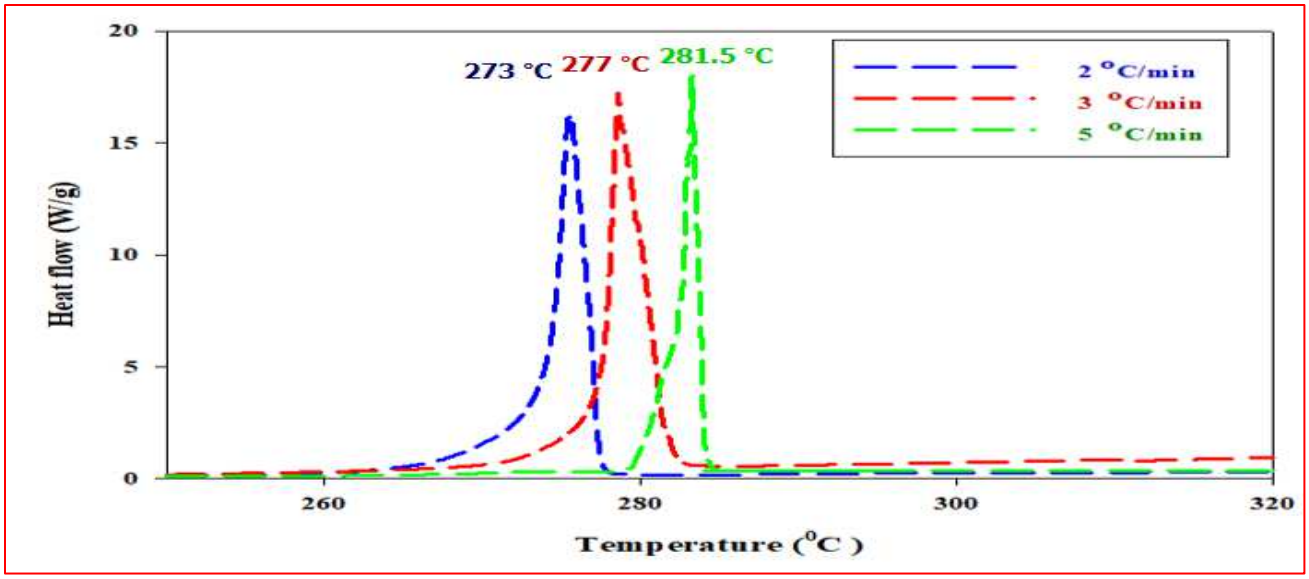

Fig. 10: DSC thermogram of different heating rates for HMX nanocomposite

It is obvious that maximum decomposition peak temperature shifts to high value with increase in heating rate [29]. The fraction reacted with temperature for different heating rates were calculated (Figure 11).

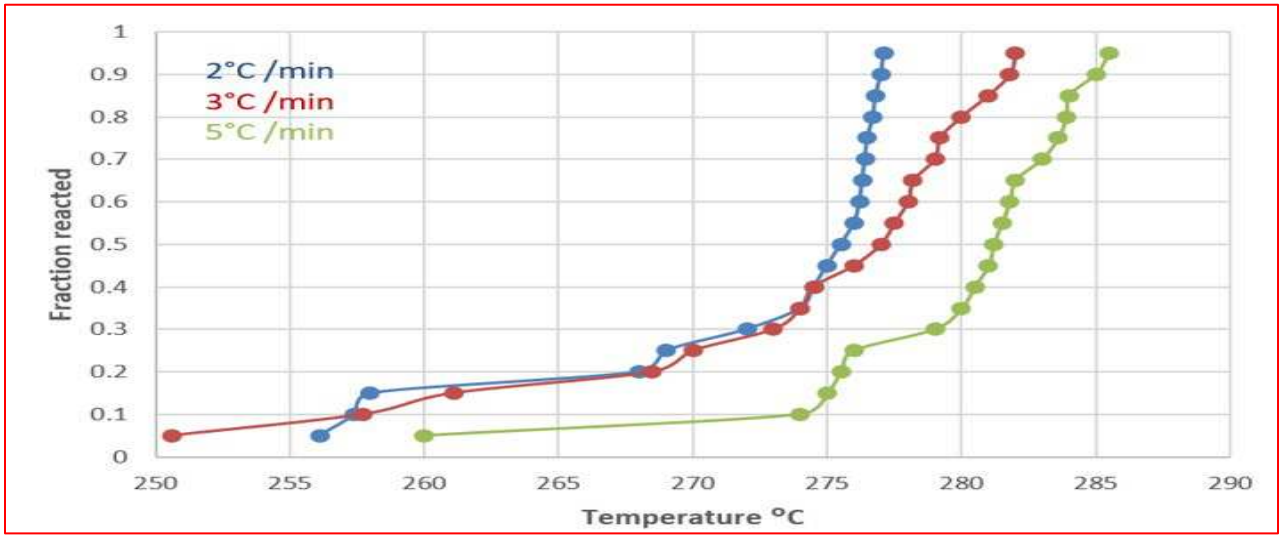

Fig. 11: Fraction reacted with temperature for different heating rates.

From the previous figure we would be able to predict the mechanism of the decomposition as indicated in the following sections.

3.4.1 Kinetic study using KAS model

The kinetic parameters obtained from the integral isoconversional method of KAS at different fraction reacted were tabulated at table (1).

Table (1) Kinetic parameters of HMX nanocomposite using KAS model

A	E_a (kJ mol^{-1})	Log A (s^{-1})	r
0.05	100.0	08.0	0.790
0.10	105.0	09.5	0.860
0.15	110.9	09.8	0.910
0.20	249.2	30.0	0.830
0.25	220.6	27.0	0.910
0.30	348.0	33.0	0.930
0.35	390.2	37.0	0.950
0.40	382.1	34.0	0.930
0.45	354.0	32.3	0.930
0.50	382.0	33.3	0.960
0.55	365.0	32.0	0.970
0.60	382.0	33.5	0.994
0.65	353.0	34.2	0.998
0.70	306.0	31.0	0.998
0.75	332.0	32.6	0.998
0.80	298.0	30.5	0.952
0.85	332.0	33.0	0.914
0.90	336.4	31.9	0.711
0.95	361.0	35.1	0.897
Mean	**281.4**	**34.3**	

The apparent activation energy of pure HMX was reported to be 376.8 KJ mol^{-1} [30]. HMX nanocomposite experienced activation energy of 281.4 kJ mol^{-1}. It can conclude that nanothermite particles experienced dramatic decrease in HMX activation energy by 23.5 %using KAs model.

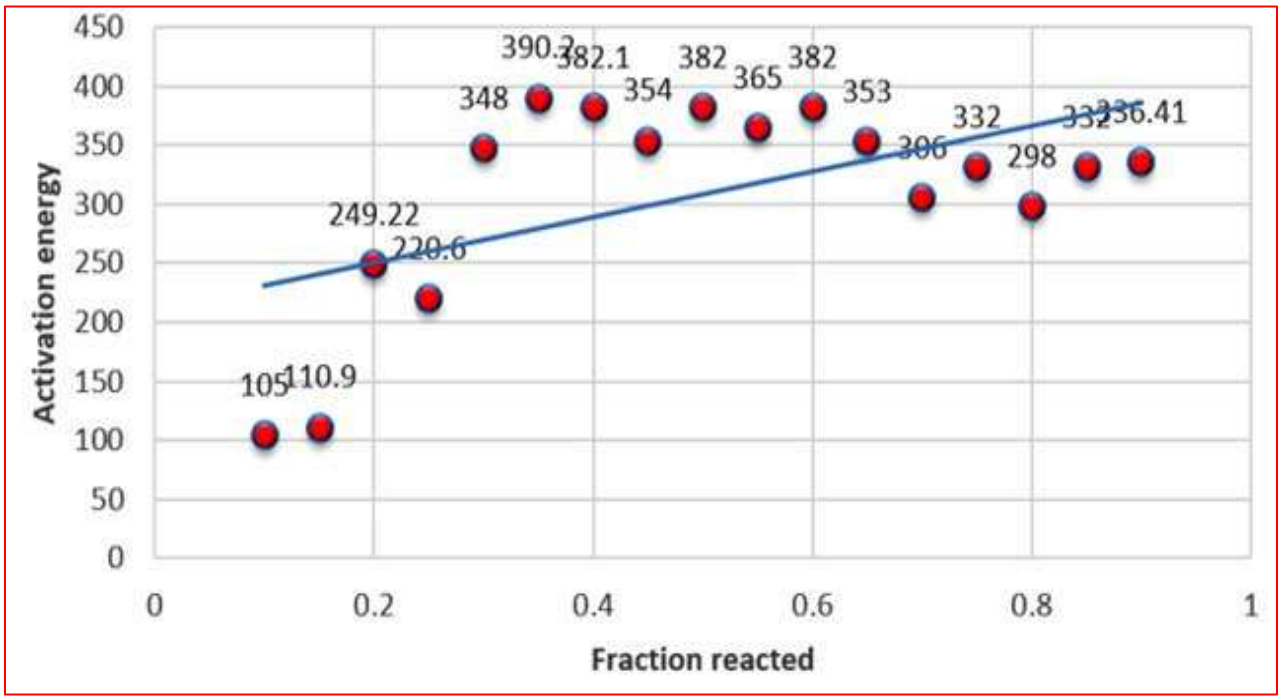

Fig. 12: Activation energy at different fraction reacted using KAS model.

In addition, the different values of the calculated activation energy at different fraction reacted are consistent. This gives confidential result of activation energy calculations.

3.4.2 Kinetic study using Kissinger model

Apparent activation energy from the Kissinger model was calculated from the slope of the straight line in (Figure 13) between, $\ln\left(\frac{\beta}{Tm,i^2}\right)$ versus $(\frac{1}{T_m})$. Apparent activation energy of HMX nanocomposite was found to be 272.82 kJ mol^{-1}.

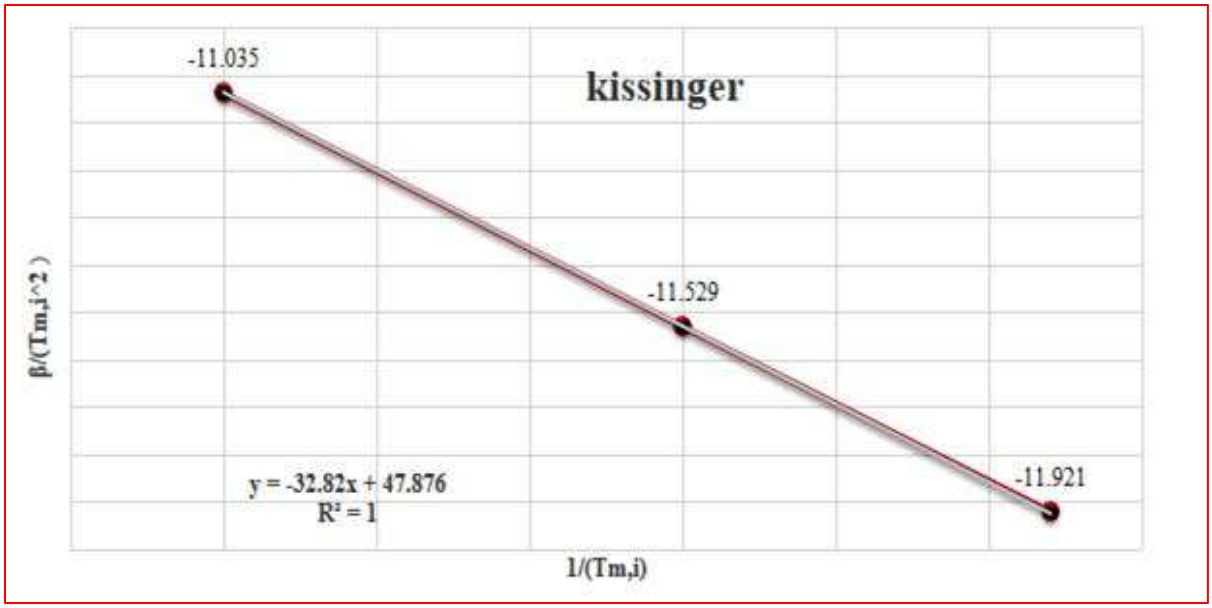

Fig. 13: Kissinger method to determine the activation energy of HMX nanocomposite.

Activation energy of pure HMX was reported to be 360.4 KJ mol^{-1} [30]. It can be concluded that nanothermite particles demonstrated dramatic change in HMX activation energy by 24.3 %. The solid-state kinetic model has been determined and it was found to fit the two-dimensional diffusion model (Figure 14). Fitting to the diffusion model could be ascribed to different crystal structure of molecules presented in the HMX nanocomposite and the diffusion process that occurs between these different crystalline structures.

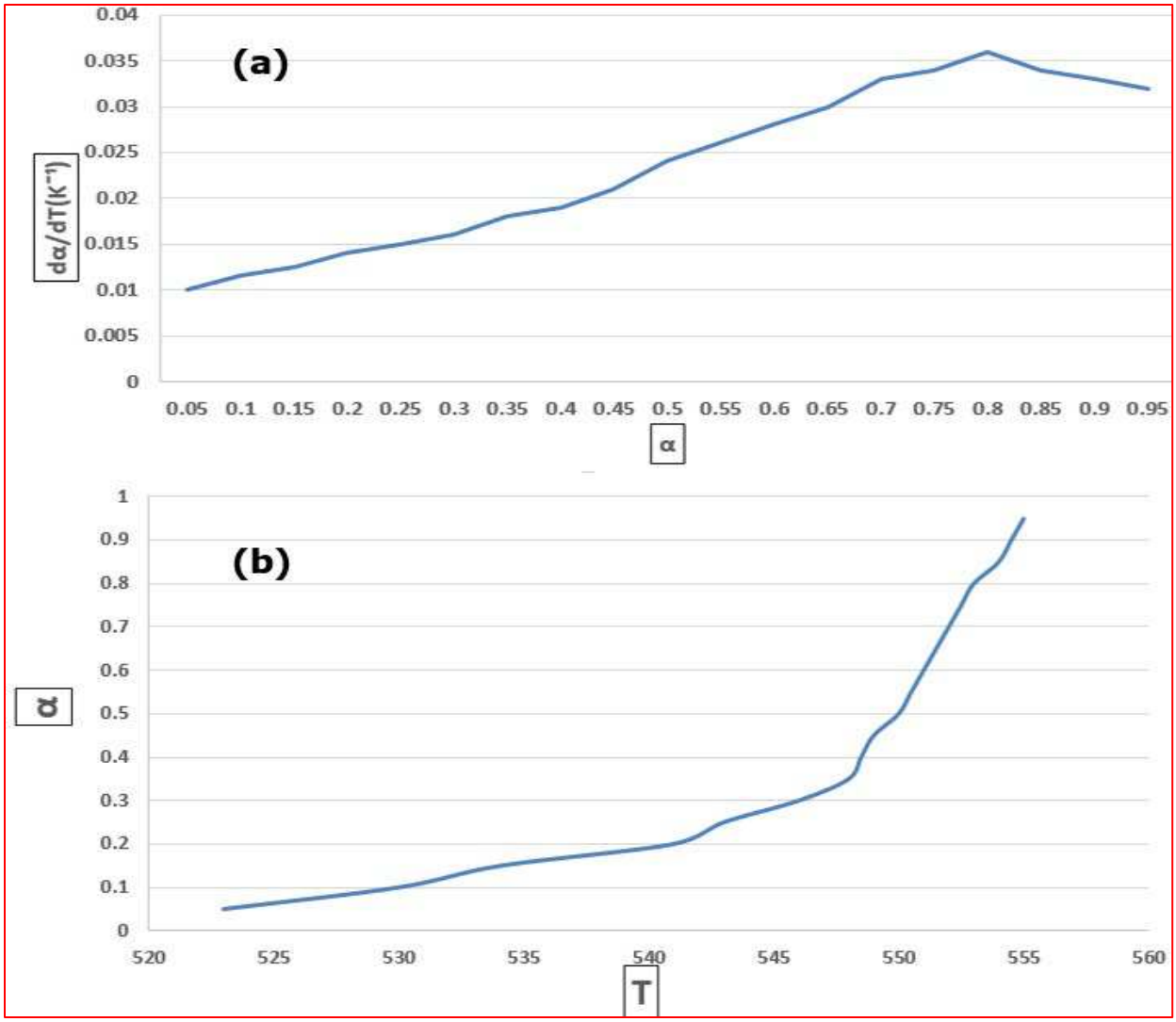

Fig. 14: Plot of α and temperature for heterogeneous decomposition reaction (a), plot of α and dα/dT for heterogeneous decomposition reaction (b).

Plot 14 was found to be in good agreement with Equations 9 and 10 for different crystalline structure.

$$\mathbf{f(\alpha) = -[\frac{1}{\ln(1-\alpha)}]} \qquad \mathbf{(9)}$$

$$\mathbf{g(\alpha) = ((1-\alpha)\ln(1-\alpha)) + \alpha} \qquad \mathbf{(10)}$$

Heterogeneous solid phase reaction was accurately modelled and the result was in a good accord with KAS and Kissinger kinetic models. For solid state reactants, Thadani reported that reduction in onset

temperature would result a lower activation energy and a higher reaction rate [31]. The integration of nanothermite particles into HMX demonstrated dramatic decrease in HMX activation energy by 23.5% and 24.3% using KAs and Kissinger models respectively. The catalytic effect of nanothermite particles can be correlated to the hydrous surface of ferric oxide particles. The surface hydroxyl groups could be released at low temperature; active ȮH radicals would attack HMX heterocyclic ring and abstract hydrogen atom from HMX heterocyclic ring (Figure 15) [12].

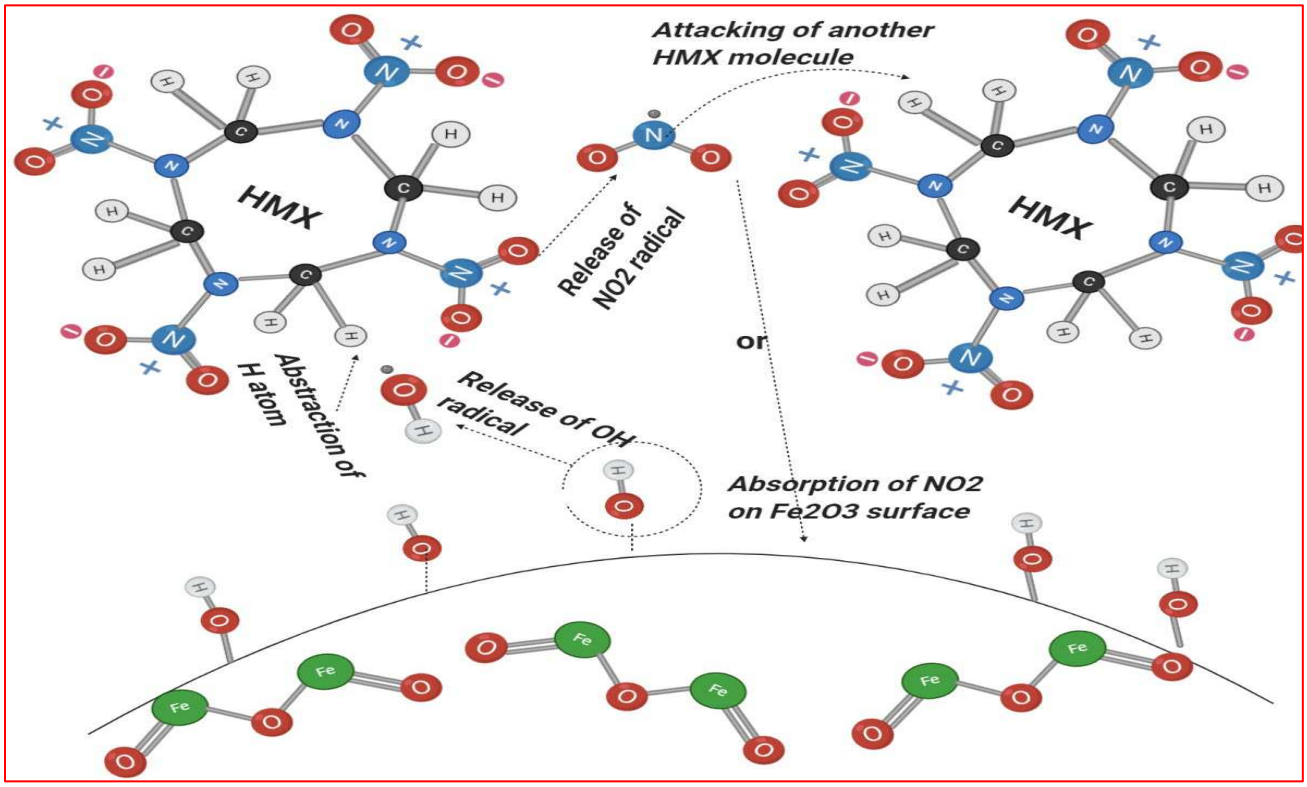

Fig. 15: HMX decomposition mechanism [32].

As a result of hydrogen abstraction, energy of the N-NO_2 bond would decrease and the nitro group would be released easily [33]. Furthermore, the released nitro group could attack another HMX molecule or absorbed on the surface of the nanoparticles with an increase in reaction exothermicity [34].

4. Conclusions

In our study colloidal Fe_2O_3 nanoparticles was fabricated by hydrothermal synthesis. The fabricated nanoparticles demonstrated 5nm size. HMX nanocomposite was developed by co-precipitation technique. Nanothermite particles demonstrated dramatic change in HMX decomposition with an increase in decomposition enthalpy by 63 %. Nanothermite particles demonstrated dramatic change in HMX decomposition kinetics. The apparent activation energy was reduced by 23.5% for isoconversional method of KAS and by 24.3% for the Kissinger method and this result confirmed the catalytic effect of the nano-additives.

5. References

1. Talawar, M., et al., *New directions in the science and technology of advanced sheet explosive formulations and the key energetic materials used in the processing of sheet explosives: Emerging trends.* Journal of hazardous materials, 2015. **300**: p. 307-321.
2. Elbasuney, S. and G.S. El-Sayyad, *The potentials of TiO2 nanocatalyst on HMX thermolysis.* Journal of Materials Science: Materials in Electronics, 2020. **31**(17): p. 14930-14940.
3. Elbasuney, S., et al., *Multi-component nanocomposite infrared flare with superior infrared signature via synergism of nanothermite and reduced graphene oxide.* Journal of Materials Science: Materials in Electronics, 2020. **31**(14): p. 11520-11526.
4. Meyer, R., J. Kohler, and A. Homburg, eds. *EXPLOSIVES*. Sixth ed. 2007, WILEY: Weinheim.
5. Fischer, N., et al., *Pushing the limits of energetic materials–the synthesis and characterization of dihydroxylammonium 5, 5′-bistetrazole-1, 1′-diolate.* Journal of Materials Chemistry, 2012. **22**(38): p. 20418-20422.
6. Elbasuney, S. and M. Yehia, *Ammonium Perchlorate Encapsulated with TiO2 Nanocomposite for Catalyzed Combustion Reactions.* Journal of Inorganic and Organometallic Polymers and Materials, 2019. **29**(4): p. 1349-1357.

7. Elbasuney, S. and M. Yehia, *Ferric Oxide Colloid: A Novel Nano-catalyst for Solid Propellants.* Journal of Inorganic and Organometallic Polymers and Materials, 2020. **30**(3): p. 706-713.
8. Huang, H., Y. Shi, and J. Yang, *Thermal characterization of the promising energetic material TKX-50.* Journal of Thermal Analysis and Calorimetry, 2015. **121**(2): p. 705-709.
9. Elghafour, A.M.A., et al., *Highly energetic nitramines: A novel platonizing agent for double-base propellants with superior combustion characteristics.* Fuel, 2018. **227**: p. 478-484.
10. Elbasuney, S., et al., *Novel High Energy Density Material Based on Metastable Intermolecular Nanocomposite.* Journal of Inorganic and Organometallic Polymers and Materials, 2020. **30**(10): p. 3980-3988.
11. Elbasuney, S., et al., *Ferric oxide colloid: novel nanocatalyst for heterocyclic nitramines.* Journal of Materials Science: Materials in Electronics, 2021.
12. Elbasuney, S., et al., *Facile synthesis of RGO-Fe2O3 nanocomposite: A novel catalyzing agent for composite propellants.* Journal of Materials Science: Materials in Electronics, 2020. **31**(23): p. 20805-20815.
13. Elbasuney, S., *Dispersion characteristics of dry and colloidal nano-titania into epoxy resin.* Powder Technology, 2014. **268**(0): p. 158-164.
14. Elbasuney, S., *Continuous hydrothermal synthesis of AlO(OH) nanorods as a clean flame retardant agent.* Particuology, 2015. **22**: p. 66-71.
15. Elbasuney, S., *Surface engineering of layered double hydroxide (LDH) nanoparticles for polymer flame retardancy.* Powder Technology, 2015. **277**: p. 63-73.
16. Cabanas, A., et al., *A continuous and clean one-step synthesis of nano-particulate Ce1− xZrxO2 solid solutions in near-critical water.* Chemical Communications, 2000(11): p. 901-902.
17. Byrappa, K. and M. Yoshimura, *Hydrothermal technology—Principles and applications.* Handbook of hydrothermal technology, 2001: p. 1-52.
18. Schäf, O., H. Ghobarkar, and P. Knauth, *Hydrothermal synthesis of nanomaterials*, in *Nanostructured Materials*. 2004, Springer. p. 23-41.
19. Gan, Y.X., et al., *Hydrothermal synthesis of nanomaterials*. 2020, Hindawi.
20. Elbasuney, S., et al., *Novel nanocomposite decoy flare based on super-thermite and graphite particles.* Journal of Materials Science: Materials in Electronics, 2020. **31**(8): p. 6130-6139.

21. Elbasuney, S., et al., *Reduced graphene oxide: a novel black body emitter for advanced infrared decoy flares.* Journal of Energetic Materials, 2020: p. 1-13.
22. Elbasuney, S., et al., *Infrared Signature of Novel Super-Thermite (Fe2O3/Mg) Fluorocarbon Nanocomposite for Effective Countermeasures of Infrared Seekers.* Journal of Inorganic and Organometallic Polymers and Materials, 2018. **28**(5): p. 1718-1727.
23. *Elbasuney, S., et al., Infrared Spectra of Customized Magnesium/Teflon/Viton Decoy Flares. Combustion, Explosion, and Shock Waves, 2019. 55(5).*
24. Elbasuney, S., et al., *Super-Thermite (Al/Fe2O3) Fluorocarbon Nanocomposite with Stimulated Infrared Thermal Signature via Extended Primary Combustion Zones for Effective Countermeasures of Infrared Seekers.* Journal of Inorganic and Organometallic Polymers and Materials, 2018. **28**.
25. Elbasuney, S., et al., *Novel (MnO2/Al) thermite colloid: an opportunity for energetic systems with enhanced performance.* Journal of Materials Science: Materials in Electronics, 2020. **31**(23): p. 21399-21407.
26. Starink, M., *The determination of activation energy from linear heating rate experiments: a comparison of the accuracy of isoconversion methods.* Thermochimica Acta, 2003. **404**(1-2): p. 163-176.
27. Kissinger, H.E., *Reaction kinetics in differential thermal analysis.* Analytical chemistry, 1957. **29**(11): p. 1702-1706.
28. Vyazovkin, S. and C. Wight, *Kinetics in solids.* Annual review of physical chemistry, 1997. **48**(1): p. 125-149.
29. Yan, Q.-L., et al., *Thermal behavior and decomposition kinetics of Formex-bonded explosives containing different cyclic nitramines.* Journal of thermal analysis and calorimetry, 2013. **111**(2): p. 1419-1430.
30. Yan, Q.-L., et al., *The influence of the semtex matrix on the thermal behavior and decomposition kinetics of cyclic nitramines.* Central European Journal of Energetic Materials, 2013. **10**(4): p. 509--528.
31. Thadhani, N.N., *Thermal analysis instrumentation for kinetics of shocked materials*. 2003, Georgia Institute of Technology.
32. ZARKO, V.E. and A.A. GROMOV, eds. *ENERGETIC NANOMATERIALS Synthesis, Characterization, and Application*. 2016, Elsevier: Amsterdam.
33. Tarver, C.M. and T.D. Tran, *Thermal decomposition models for HMX-based plastic bonded explosives.* Combustion and Flame, 2004. **137**(1-2): p. 50-62.

34. Zarko, V.E. and A.A. Gromov, *Energetic nanomaterials: Synthesis, characterization, and application*. 2016: elsevier.

Figures

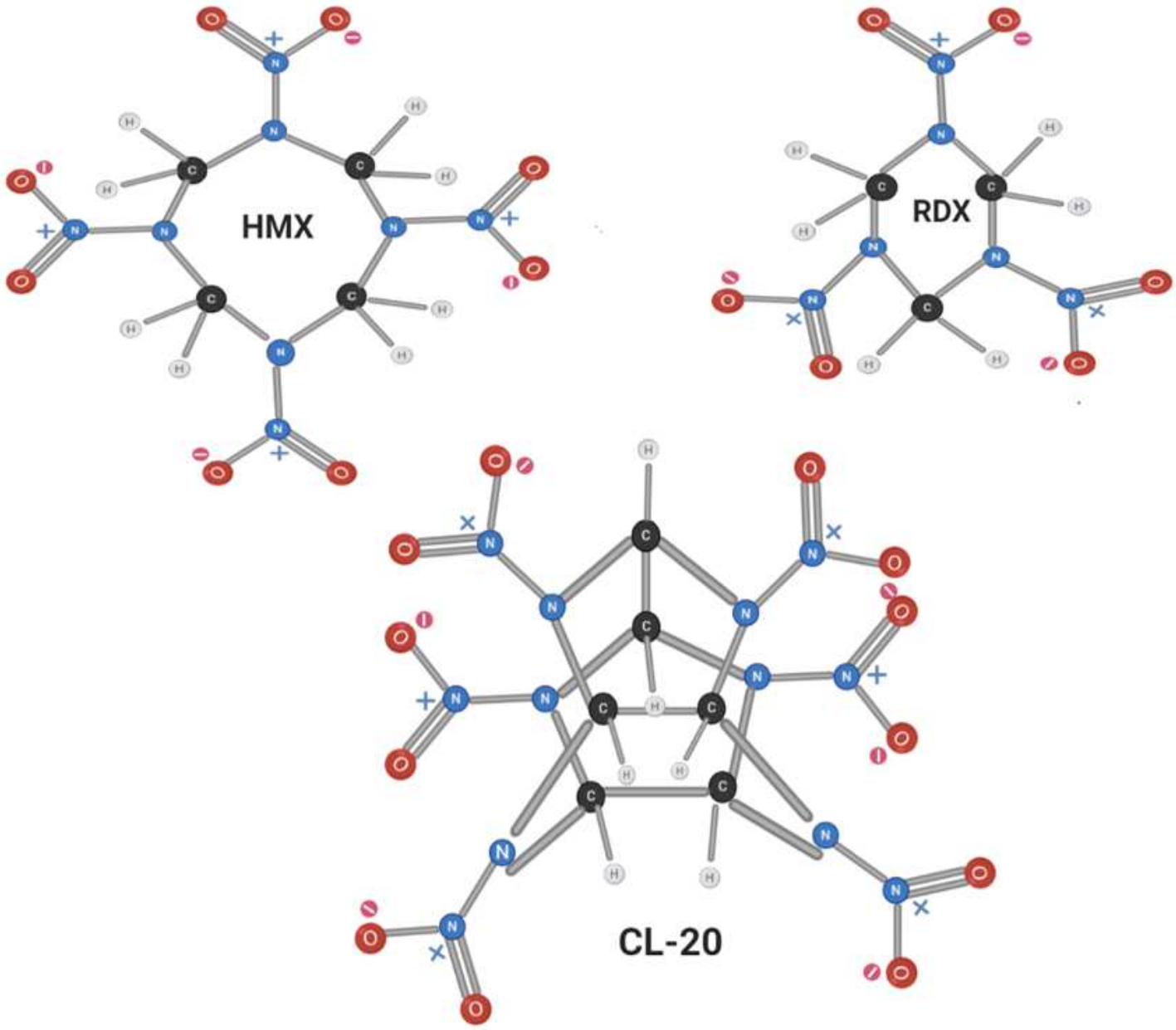

Figure 1

Chemical structure of common energetic nitramines [4].

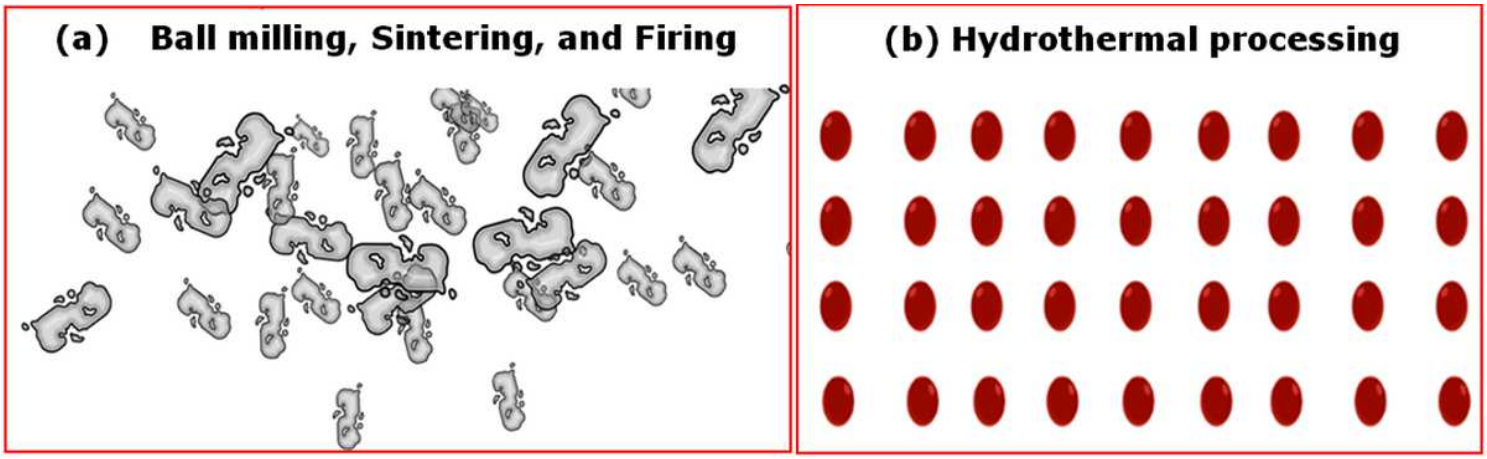

Figure 2

Nanoparticles morphology produced by different methods [13-15].

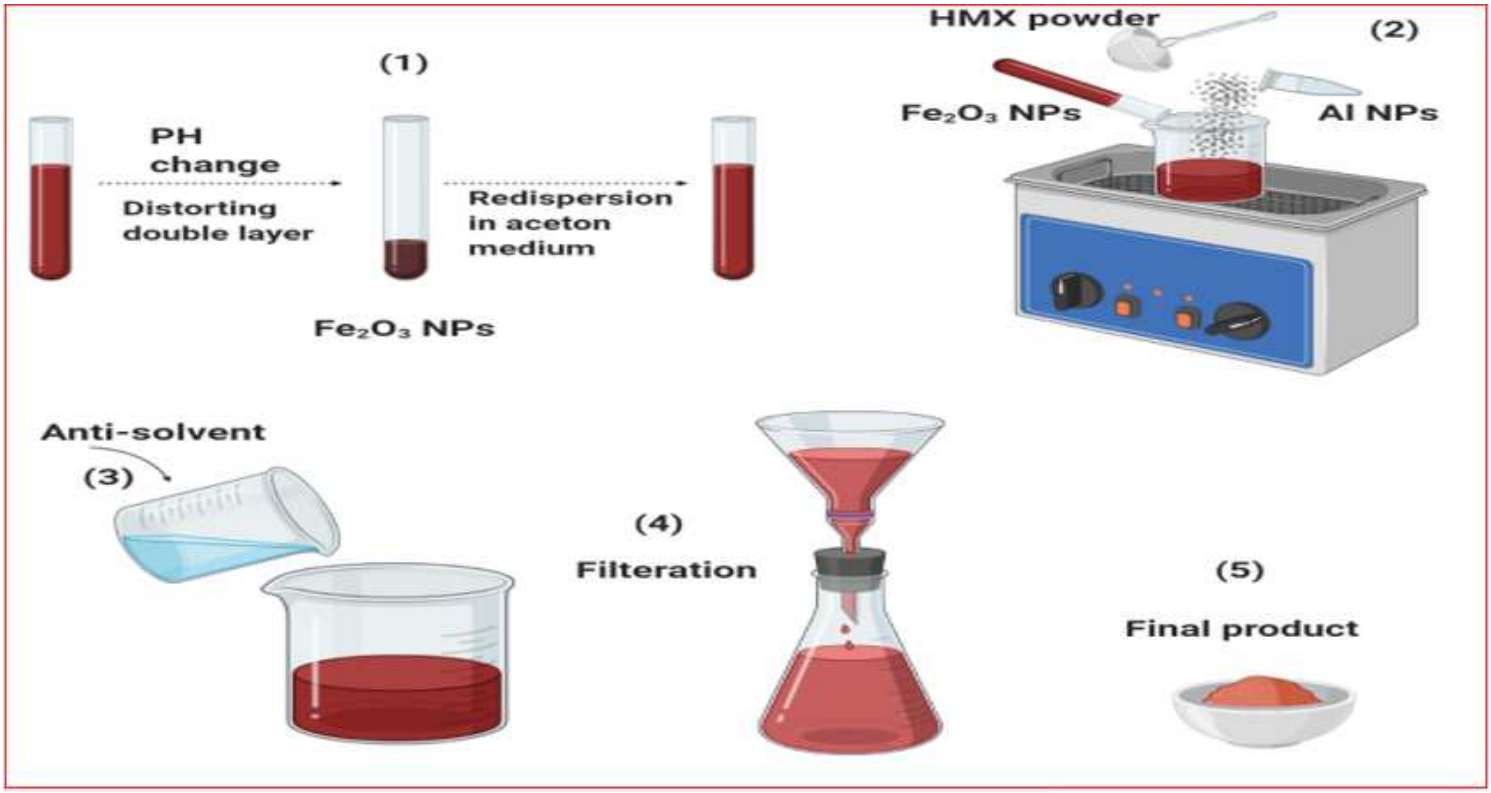

Figure 3

Solvent anti-solvent technique for preparation of HMX nanocomposite

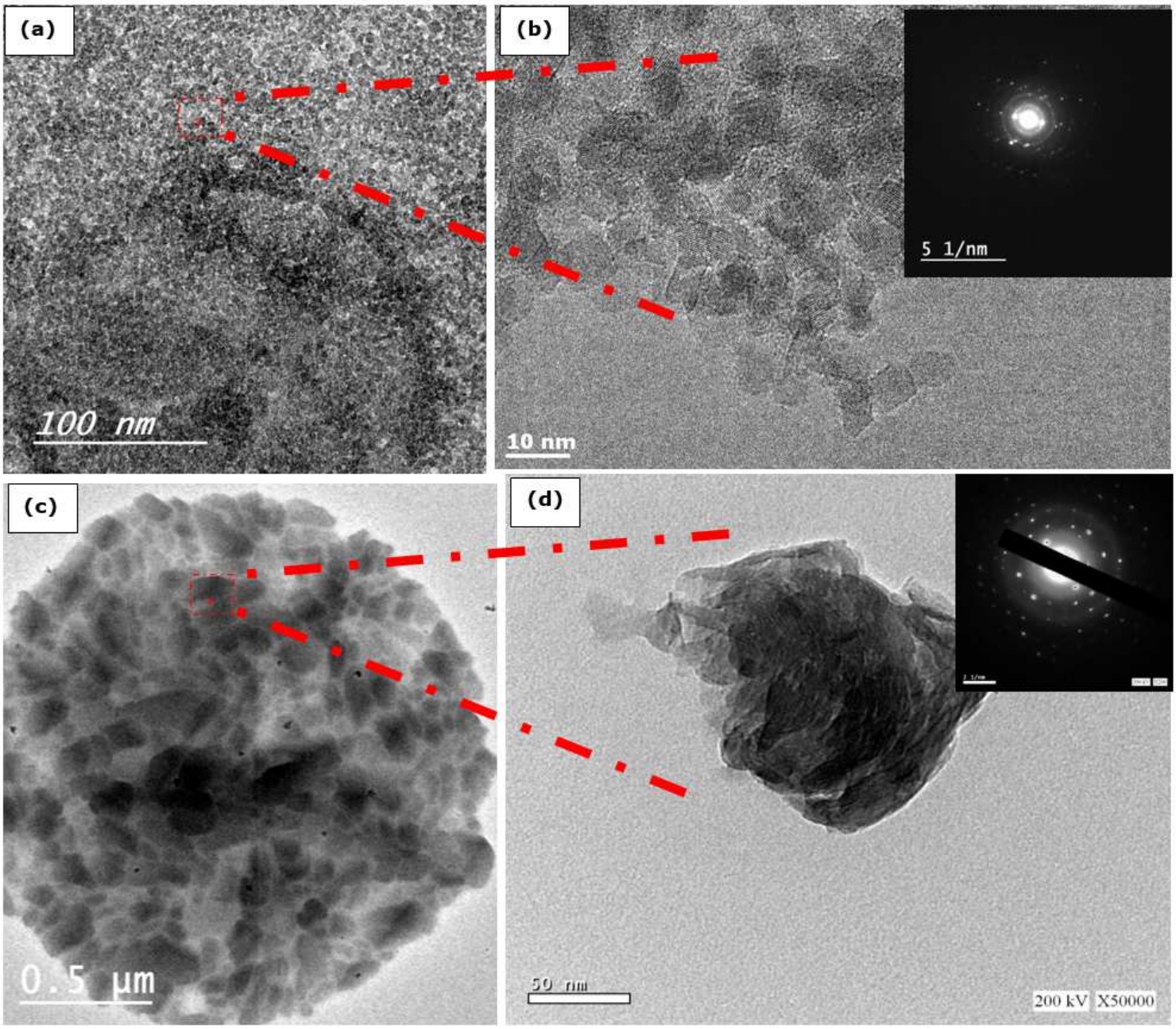

Figure 4

TEM for the synthesized Fe2O3 nanoparticles (a, b) and aluminium nanoparticles (c, d).

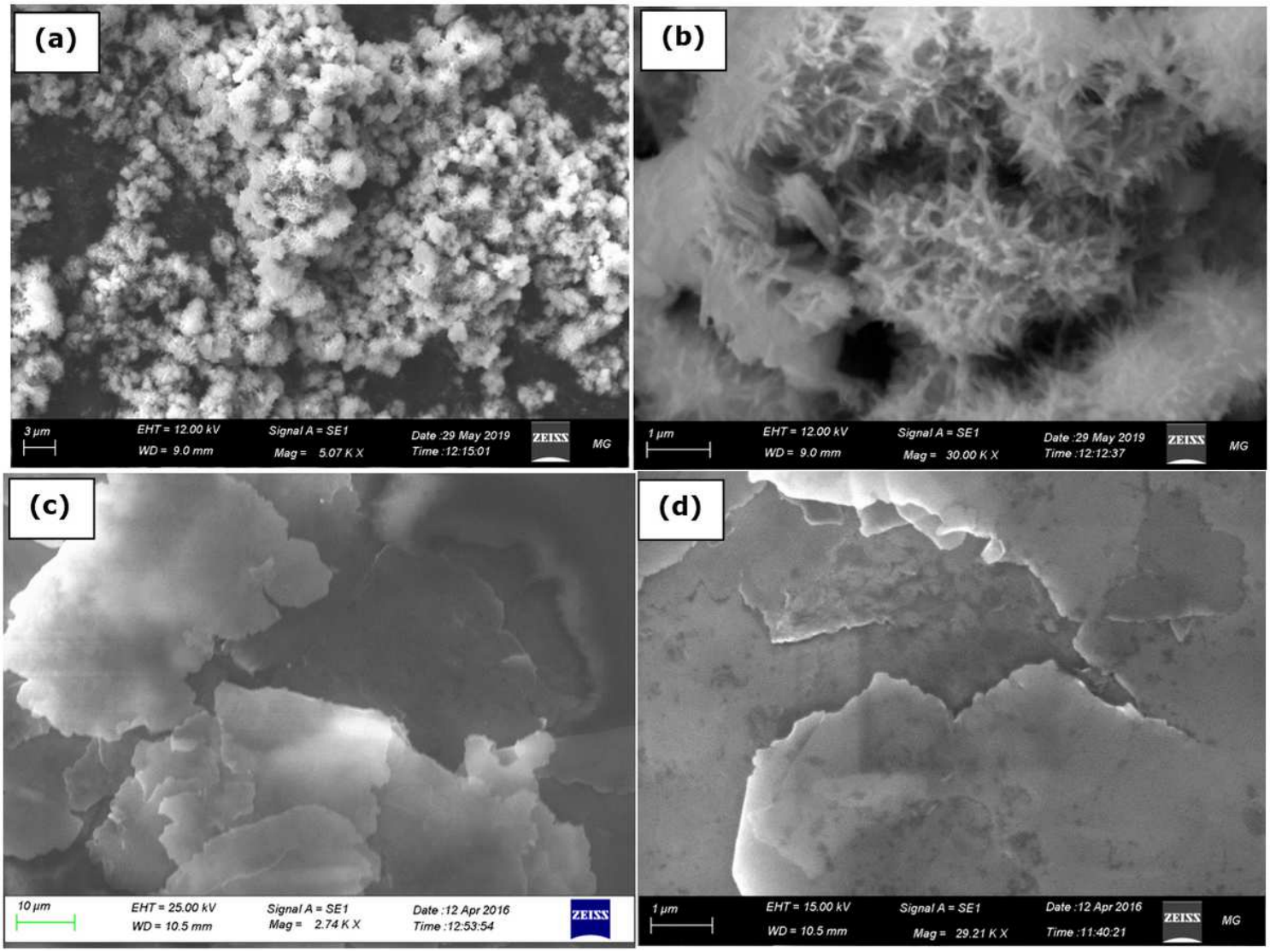

Figure 5

SEM micrograhs Fe2O3 nanoparticles (a, b), aluminium nanoplates (c, d).

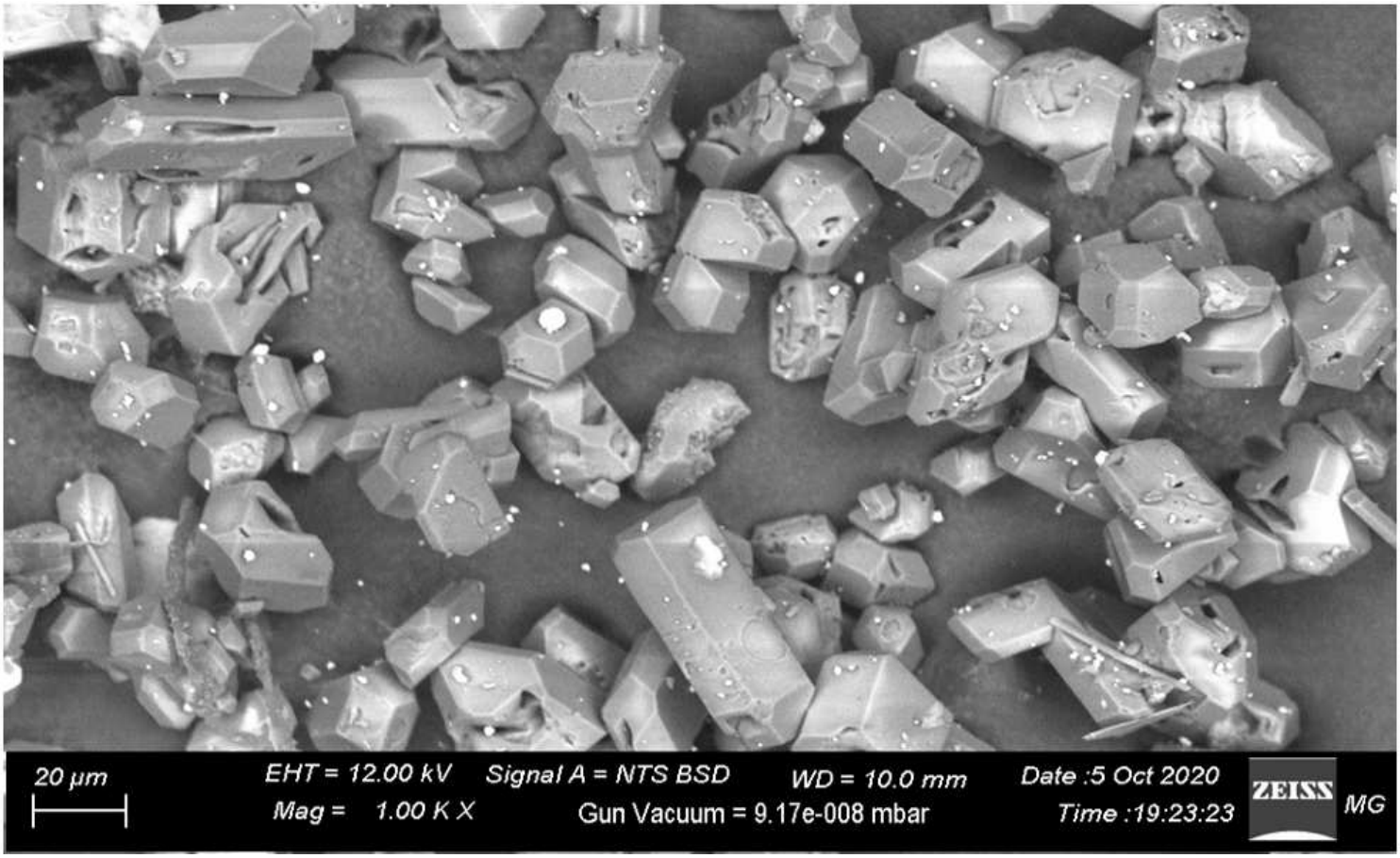

Figure 6

Morphology of HMX nanocomppsoite

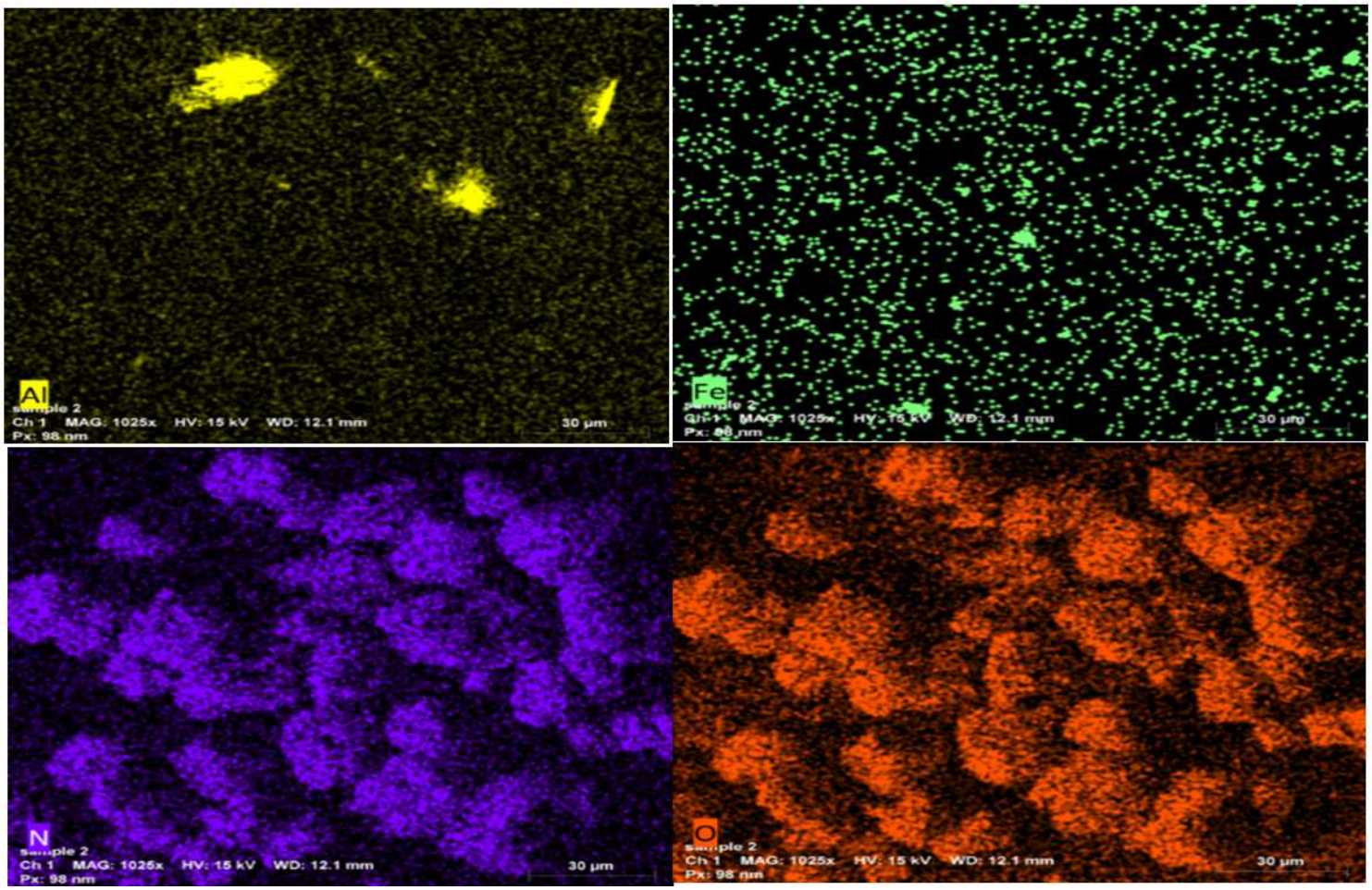

Figure 7

Elemental mapping of HMX nanocomposite

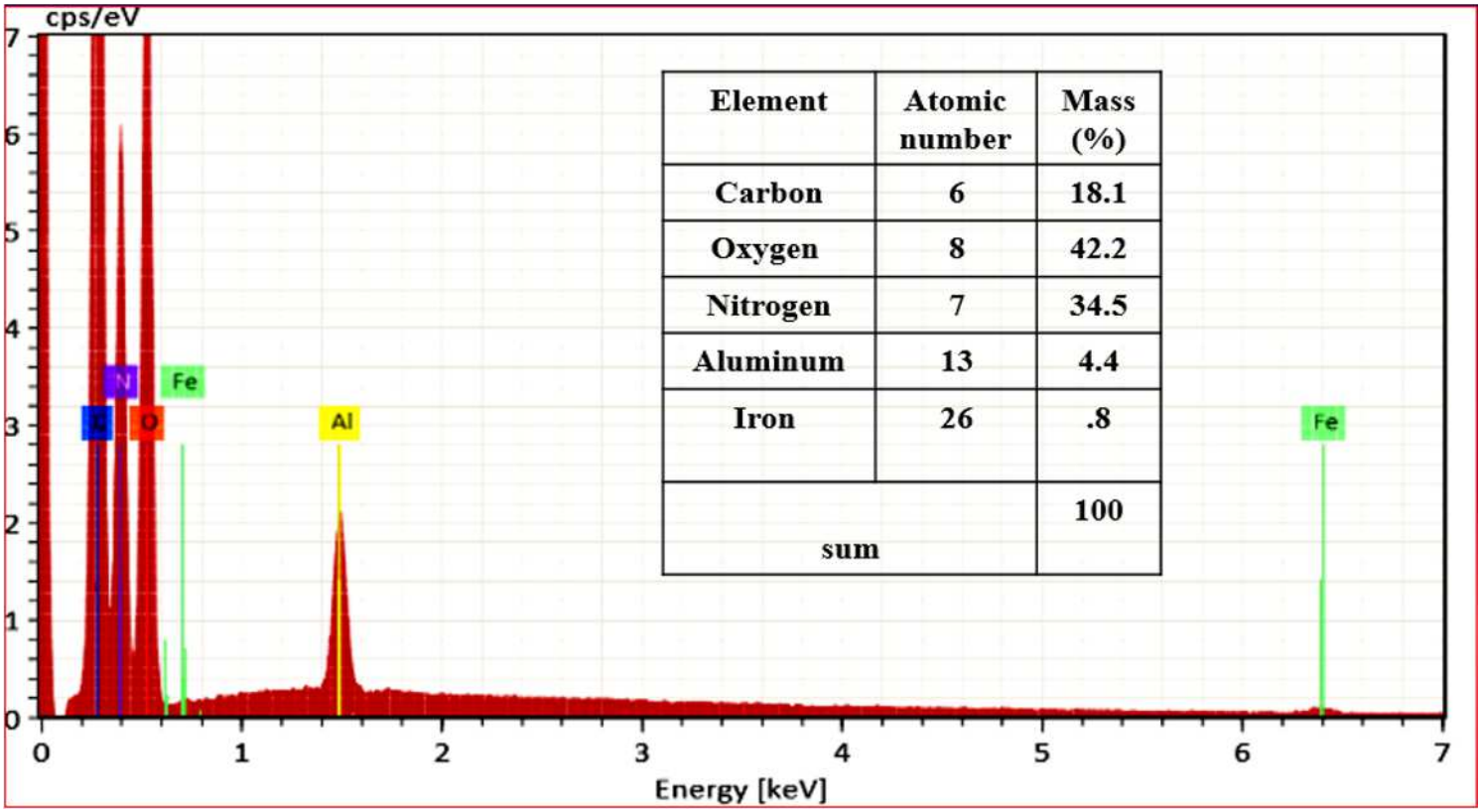

Element	Atomic number	Mass (%)
Carbon	6	18.1
Oxygen	8	42.2
Nitrogen	7	34.5
Aluminum	13	4.4
Iron	26	.8
sum		100

Figure 8

EDX elemental analysis of HMX nanocomposite.

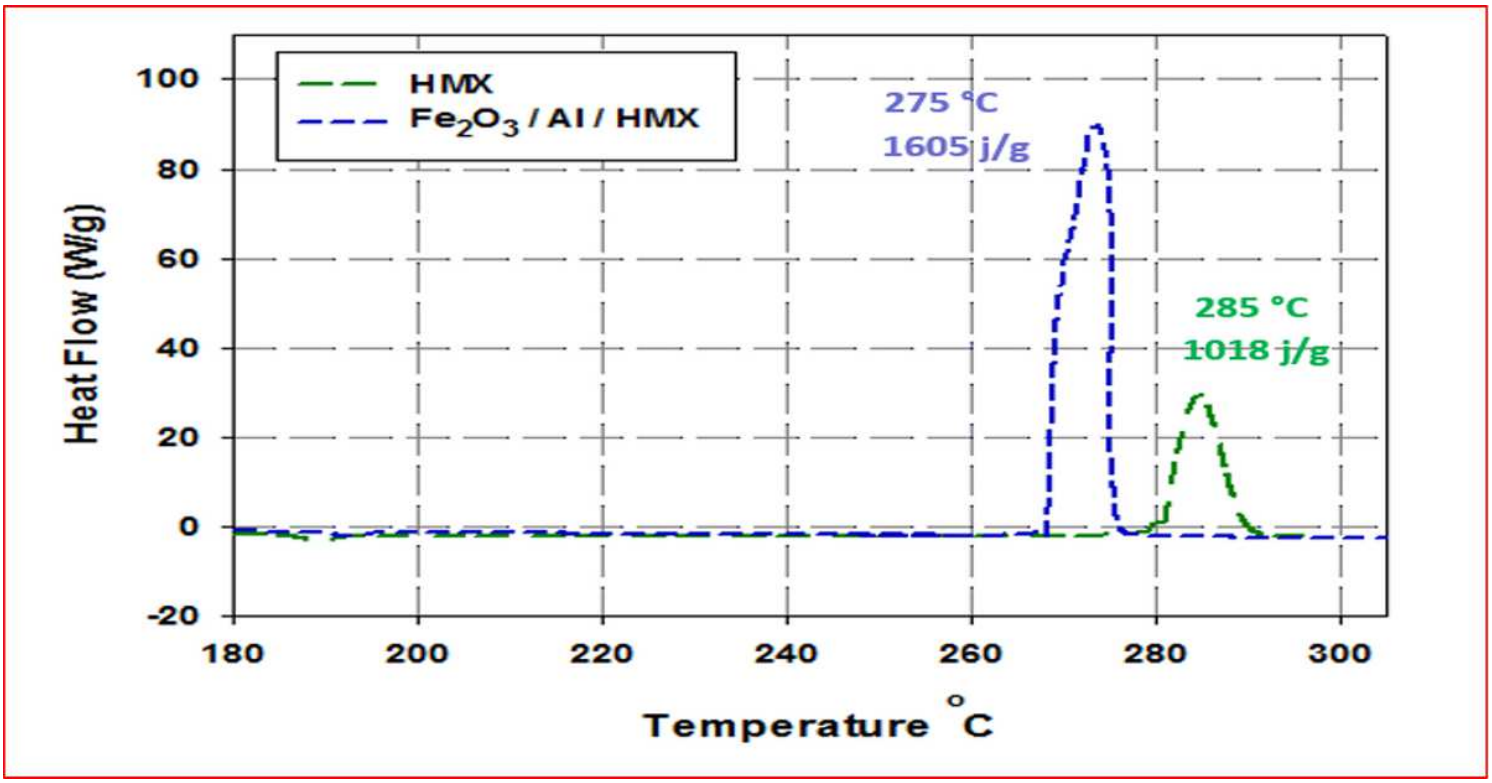

Figure 9

Impact of thermite particles on HMX thermal behaviour.

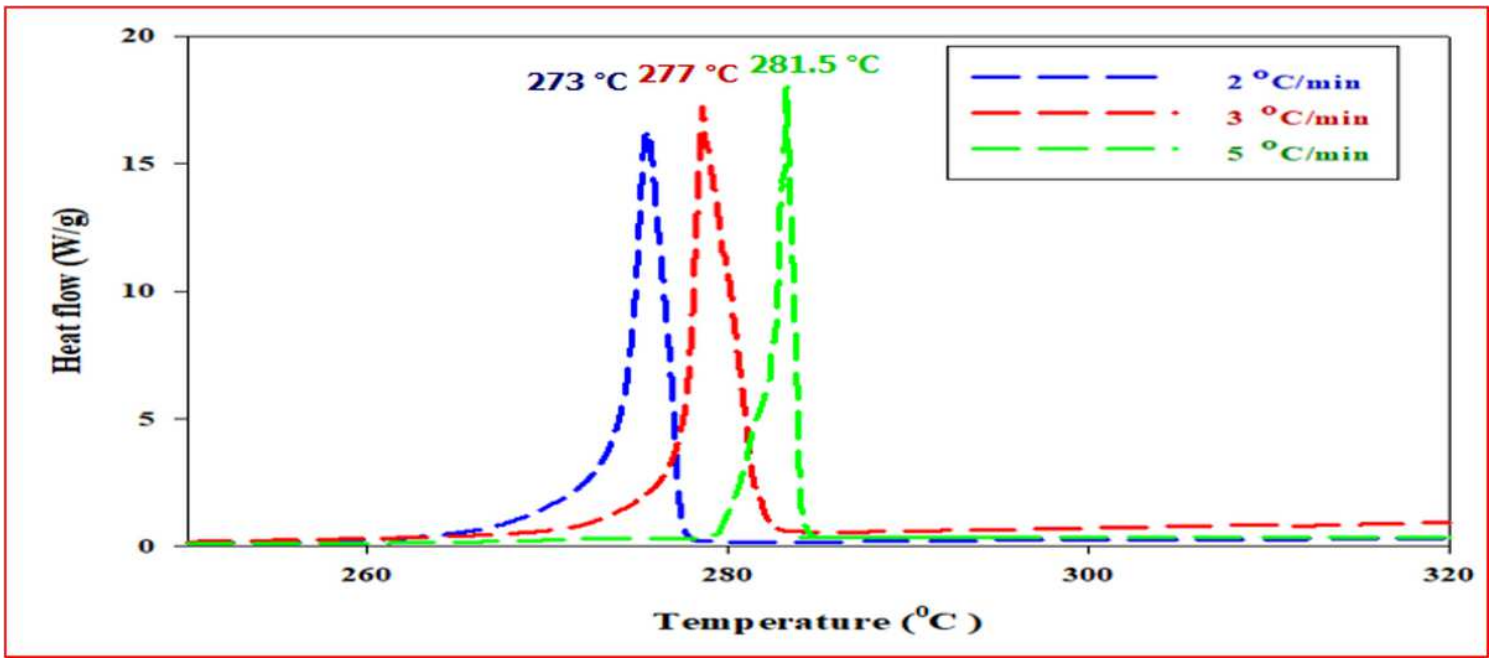

Figure 10

DSC thermogram of different heating rates for HMX nanocomposite

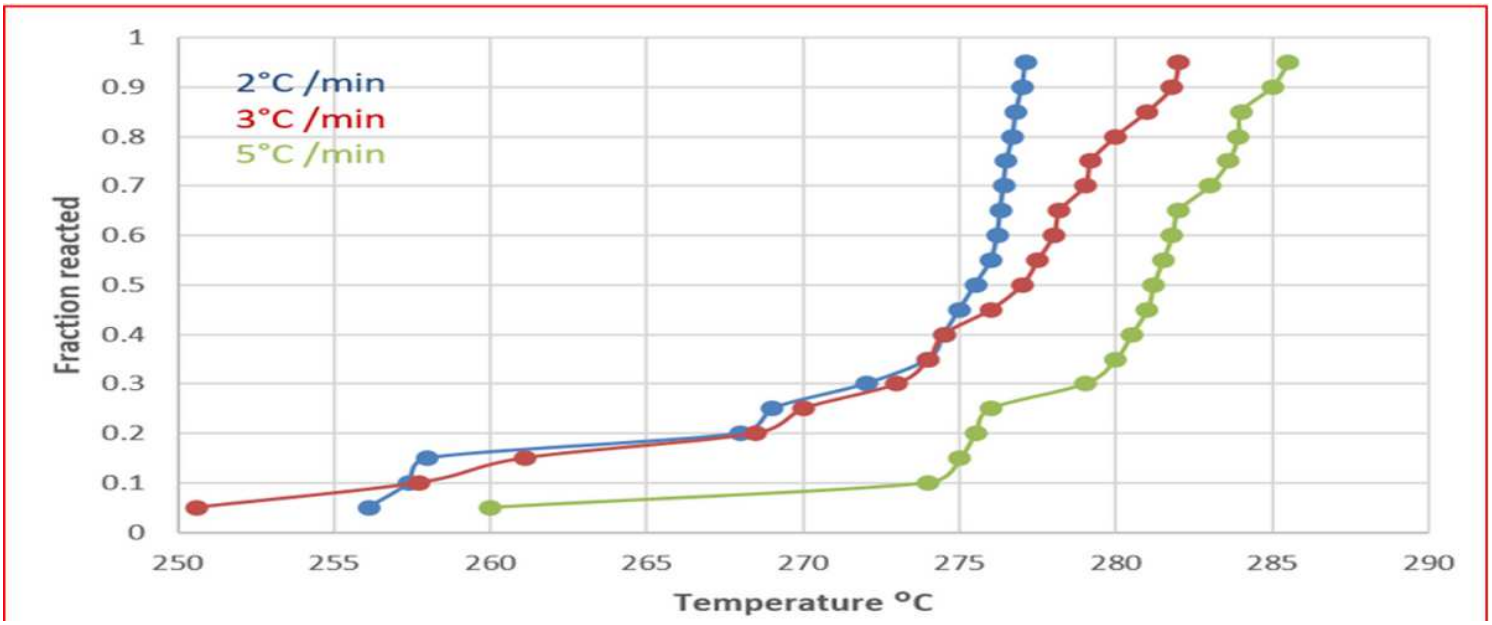

Figure 11

Fraction reacted with temperature for different heating rates.

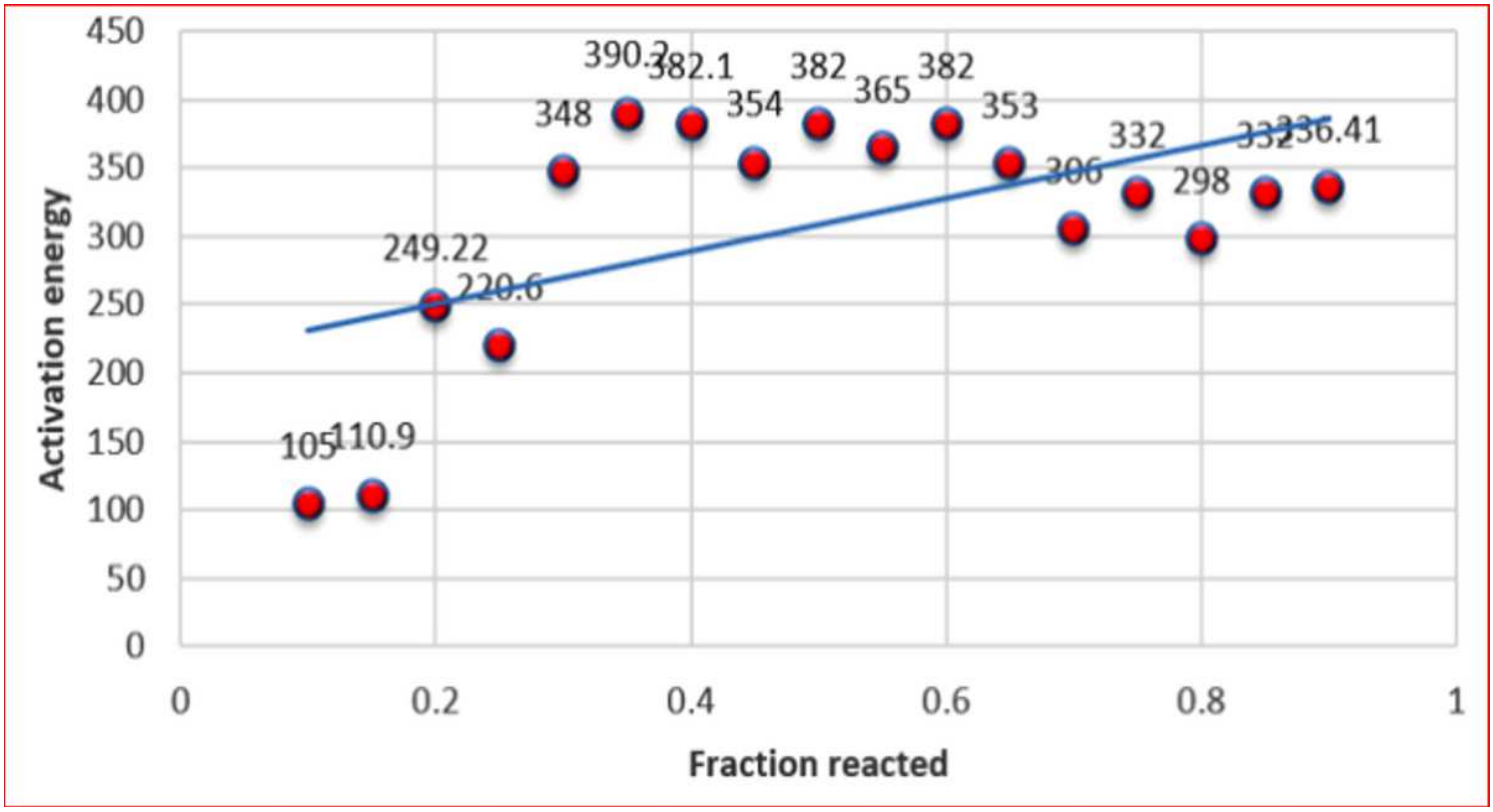

Figure 12

Activation energy at different fraction reacted using KAS model.

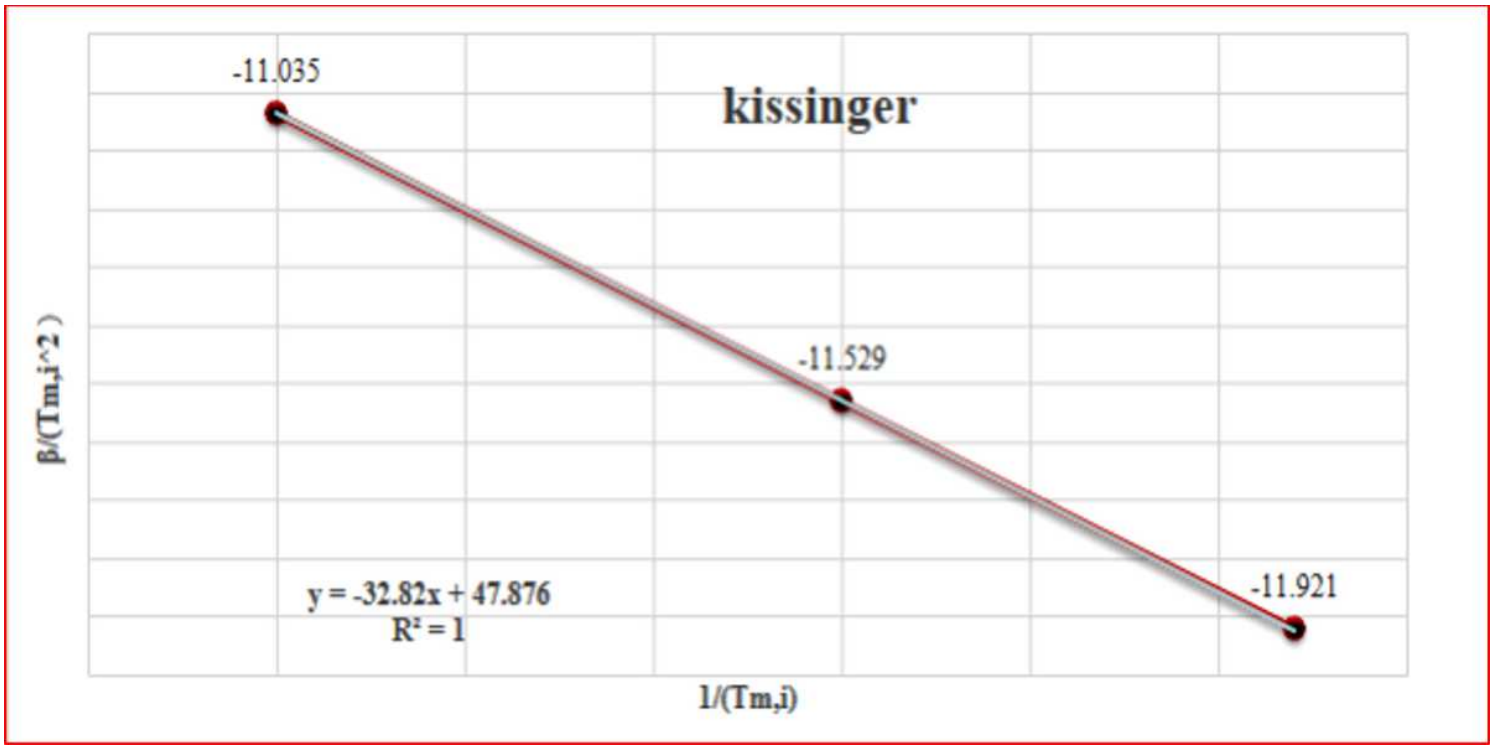

Figure 13

Kissinger method to determine the activation energy of HMX nanocomposite.

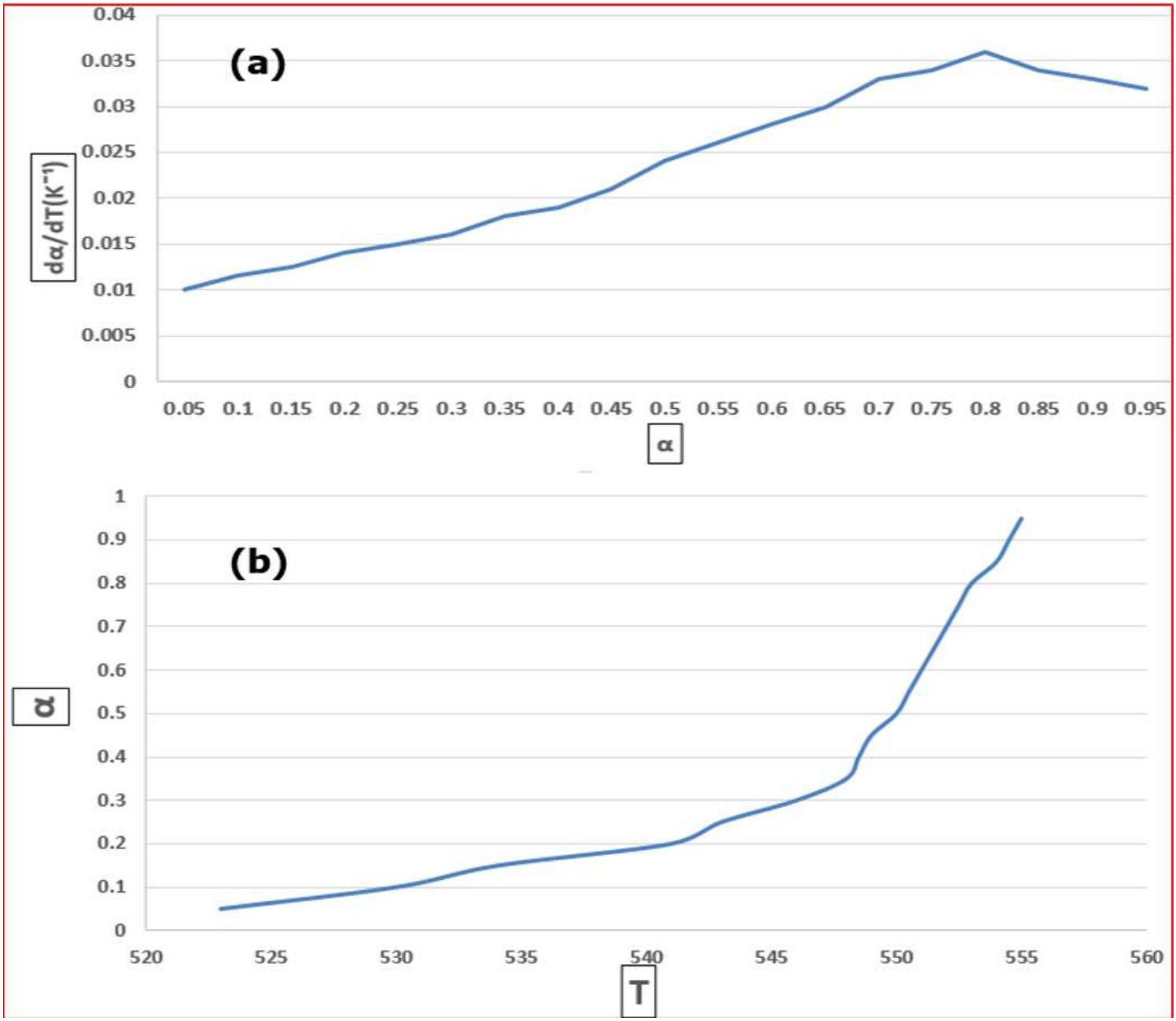

Figure 14

Plot of α and temperature for heterogeneous decomposition reaction (a), plot of α and dα/dT for heterogeneous decomposition reaction (b).

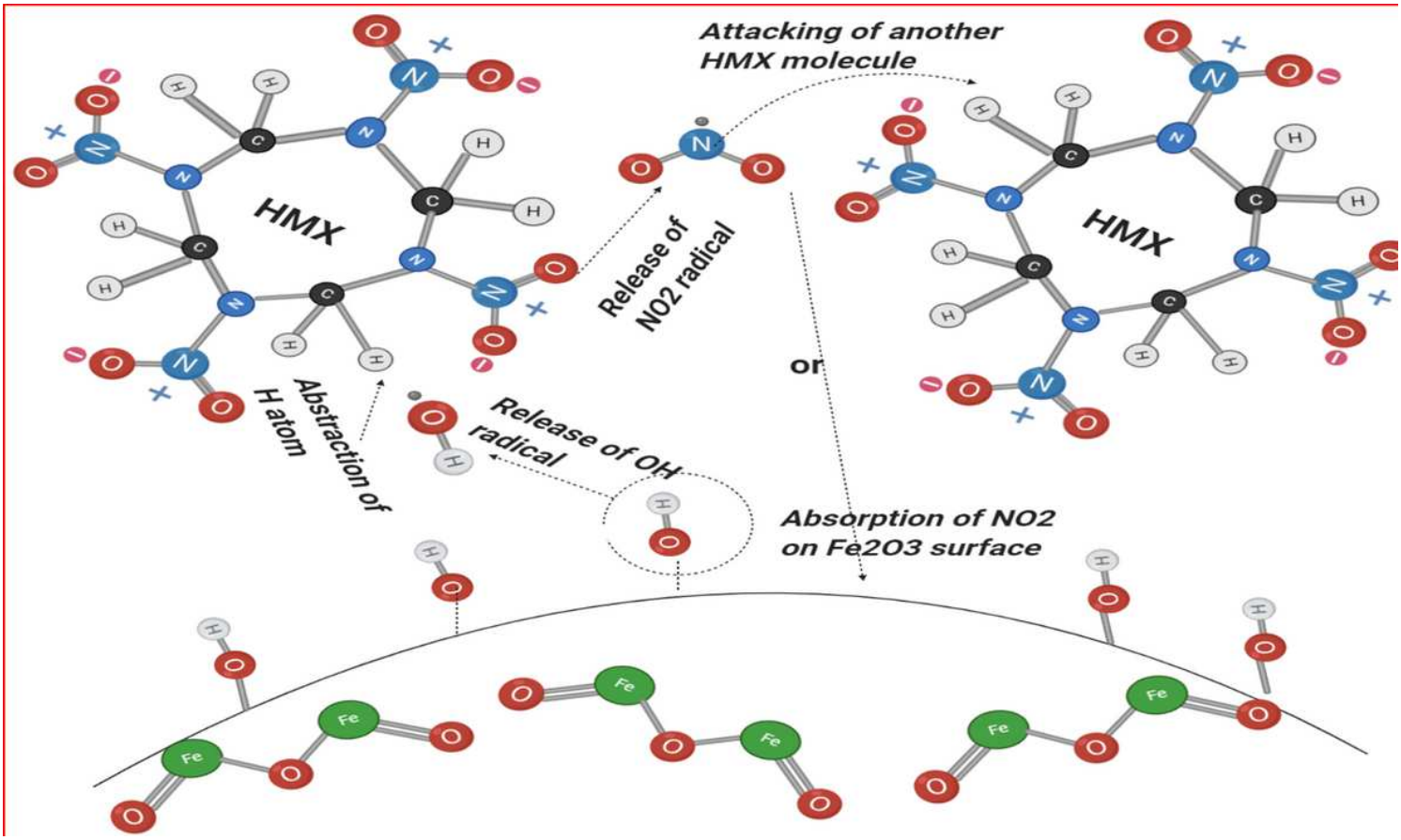

Figure 15

HMX decomposition mechanism [32].